

Crime in Philadelphia: Bayesian Clustering with Particle Optimization

Cecilia Balocchi, Sameer K. Deshpande,

Edward I. George, and Shane T. Jensen

Abstract

Accurate estimation of the change in crime over time is a critical first step towards better understanding of public safety in large urban environments. Bayesian hierarchical modeling is a natural way to study spatial variation in urban crime dynamics at the neighborhood level, since it facilitates principled “sharing of information” between spatially adjacent neighborhoods. Typically, however, cities contain many physical and social boundaries that may manifest as spatial discontinuities in crime patterns. In this situation, standard prior choices often yield overly-smooth parameter estimates, which can ultimately produce miscalibrated forecasts. To prevent potential over-smoothing, we introduce a prior that first partitions the set of neighborhoods into several clusters and then encourages spatial smoothness within each cluster. In terms of model implementation, conventional stochastic search techniques are computationally prohibitive, as they must traverse a combinatorially vast space of partitions. We introduce an ensemble optimization procedure that simultaneously identifies several high probability partitions by solving one optimization problem using a new local search strategy. We then use the identified partitions to estimate crime trends in Philadelphia between 2006 and 2017. On simulated and real data, our proposed method demonstrates good estimation and partition selection performance. Supplementary materials for this article are available online.

Keywords: Variational inference, Bayesian Model Averaging, urban analytics, spatial clustering, boundary detection, spatial smoothness.

1 Introduction

Accurate modeling of urban crime dynamics benefits many constituents: law enforcement officials can make more informed decisions about how to deploy resources to ensure public safety, urban planners can better understand how socio-economic factors and the built environment affect crime, and city officials can develop community programs and interventions to improve the overall quality of life in the city. In this paper, we study how crime has evolved in the city of Philadelphia between 2006 and 2017 with a focus on finding clusters of neighborhoods with similar crime dynamics.

Bayesian hierarchical modeling is a very natural way to study crime at the neighborhood level as it allows us to “borrow strength” between spatially adjacent neighborhoods. In fact, [Balocchi and Jensen \(2019\)](#) have demonstrated that Bayesian models that encourage spatial shrinkage can yield more accurate predictions than models that do not introduce dependencies between parameters from adjacent neighborhoods. Following that work, we propose a model that extends [Bernardinelli et al. \(1995\)](#)’s linear model to crime incidents with spatially varying intercepts (mean level of crime) and spatially varying slopes (time trend).

Priors based on conditionally auto-regressive (CAR) models ([Besag, 1974](#)) are workhorses in the Bayesian spatial statistics literature that encourage shrinking each neighborhood’s parameters towards the average value of the parameters from adjacent neighborhoods. Though these models are an intuitive and popular way to “share information” between spatially adjacent regions, they can introduce a level of smoothness at odds with the realities of complex urban environments. In fact, as we will see in [Section 2](#), while crime incidents in Philadelphia display considerable spatial correlation, there are also many sharp spatial discontinuities. This is because geographic aspects of the city, such as major streets, parks, and rivers, and latent socioeconomic divisions can create barriers that may be associated with discontinuities in crime patterns.

In the context of crime modeling, using a CAR prior without accounting for potential discontinuities can lead to poor estimation of crime around these geographic or socioeconomic barriers. Although manually adjusting the CAR prior to prevent smoothing over these boundaries is conceptually simple, it presupposes knowledge about the location of these discontinuities, which are often latent or unknown. A far more elegant and agnostic approach is to use the data itself to identify the discontinuities.

There is a very rich literature on data-adaptive strategies for detecting discontinuities at the border between adjacent neighborhoods, also known as *wombling*. One approach to wombling involves first fitting a simple model that does not account for potential discontinuities and then identifying jumps in the fitted values (see, e.g., [Boots \(2001\)](#), [Li et al. \(2011\)](#), [Banerjee et al. \(2012\)](#), [Lu and Carlin \(2005\)](#), and [Lee and Mitchell \(2013\)](#)). Alternatively, many authors directly model uncertainty about which borders correspond to sharp discontinuities within larger Bayesian hierarchical models (see, e.g., [Lee and Mitchell \(2012\)](#), [Lu et al. \(2007\)](#), and [Balocchi and Jensen \(2019\)](#)). While directly modeling the uncertainty in discontinuity locations is intuitively appealing, these latter models are heavily over-parametrized; in fact, they introduce one latent parameter for each pair of adjacent neighborhoods.

Rather than look for individual discontinuities between pairs of neighborhoods, we instead aim to identify *clusters* of neighborhoods that exhibit similar crime dynamics. Compared to wombling, clustering encourages dimensionality reduction while maintaining model interpretability and flexibility. In this paper, we propose a “CAR-within-clusters” model where we introduce *two latent spatial partitions* of neighborhoods in Philadelphia, one for the mean levels of crime and one for the temporal trends. We then specify separate CAR priors on the neighborhood-specific parameters within each cluster of each partition. We describe our data and introduce this model in [Section 2](#).

Like similar spatial clustering approaches (see, e.g., [Knorr-Held and Raßer \(2000\)](#), [Denison and Holmes \(2001\)](#), [Feng et al. \(2016\)](#), and references therein), we treat parameters arising from different clusters independently *a priori*. However, unlike these works, we do not assume that all parameters within a cluster are equal. Instead, we allow the parameters to vary smoothly within each cluster. Our approach combines positive aspects of clustering and wombling: we are able to find areas displaying different crime dynamics and simultaneously interpret borders between clusters as barriers corresponding to spatial discontinuities.

In our implementation, we have three primary tasks: (i) identify the two underlying spatial partitions, (ii) estimate the neighborhood-level parameters, and (iii) make predictions of future crime incidents while accounting for our uncertainty about the partitions. These goals are complicated by the combinatorial vastness of the latent product space of spatial partitions, rendering typical stochastic search techniques computationally prohibitive. We instead focus on posterior optimization. However, rather than simply finding the *maximum a posteriori* (MAP) partitions, we propose an extension of [Ročková \(2018\)](#)’s ensemble optimization framework that simultaneously identifies multiple partitions with high posterior probability

by solving a *single* optimization problem. In Section 3, we show that solving this problem is formally equivalent to finding a particular variational approximation of the discrete posterior distribution of the pairs of partitions. We introduce a new local search strategy that, at a high level, runs several greedy searches that are made “mutually aware” by an entropy penalty. This penalty promotes diversity among the estimated partitions by discouraging different search paths from visiting the same point in the latent discrete space. By identifying several high posterior probability partitions we can easily incorporate uncertainty about the latent clusterings into our estimation of the parameters and prediction, with Bayesian Model Averaging (BMA; Raftery et al. (1997)). In Section 4, we illustrate our proposed methodology on simulated data before applying it to the Philadelphia data in Section 5. We conclude with a discussion of our results and an outline of potential future directions in Section 6. A software implementation of our method and all code and data to replicate the results in this paper are available at github.com/cecilia-balocchi/particle-optimization.

2 Data and the “CAR–within–clusters” Model

For the first time in decades, Philadelphia is experiencing population growth and its built environment is rapidly evolving; this transformation makes it an interesting real-time case study for examining how crime evolves over time. Our crime data comes from opendataphilly.org, where the Philadelphia Police Department publicly releases the location, time, and type of each reported crime in the city. While there has been an overall decrease in the total amount of crime in the city over the last decade, we can obtain a more nuanced understanding by examining the temporal trends at a local neighborhood level. Our analysis focuses on *violent* crimes, which include homicides, rapes, robberies, and aggravated assaults (FBI, 2011), aggregated at the census tract level. In all, Philadelphia is divided into $N = 384$ census tracts, which we treat as large neighborhoods in our analysis, as census tracts contain approximately 4,000 inhabitants each.

For the years between 2006 ($t = 0$) and 2017 ($t = 11$), let $c_{i,t}$ be the total number of violent crimes reported in tract i during year t . The distribution of crime counts $c_{i,t}$ displays considerably skewness. Similar to Balocchi and Jensen (2019), rather than modeling $c_{i,t}$ directly, we work with an inverse hyperbolic sine transformation (Burbidge et al., 1988) of

the violent crime counts:

$$y_{i,t} = \log \left(c_{i,t} + (c_{i,t}^2 + 1)^{1/2} \right) - \log(2).$$

This transformation is a close approximation of $\log(c_{i,t})$ but is also well-defined for neighborhoods that had a crime count of zero in certain years.

2.1 Model

To study the crime dynamics at the neighborhood level in Philadelphia, we consider a simple linear regression model:

$$y_{i,t} = \alpha_i + \beta_i(t - \bar{t}) + \varepsilon_{i,t}; \quad \varepsilon_{i,t} \sim N(0, \sigma^2) \quad (1)$$

where time t has been centered, so that the parameters α_i and β_i respectively represent the mean level of crime and the trend over time of crime in census tract i . Linear models are typically employed when the number of time points is small or moderate ([Bernardinelli et al., 1995](#); [Anderson et al., 2017](#)).

We can obtain an initial estimate of the average levels α_i and time trends β_i of crime by treating each neighborhood independently and computing the maximum likelihood estimates (MLEs) within each neighborhood. [Figure 1](#) displays these estimates and reveals that the broad negative time trend in crime is not uniform across the city. In fact, in a small number of neighborhoods, crime has actually increased over the last decade.

We also see in [Figure 1](#) that, with few notable exceptions, spatially adjacent neighborhoods tends to have similar MLEs, suggesting a high degree of spatial correlation in the neighborhood-level crime dynamics. We take a hierarchical Bayesian approach in order to “borrow strength” between neighborhoods that involves specifying a prior distribution on the parameters $\boldsymbol{\alpha} = (\alpha_1, \dots, \alpha_N)$ and $\boldsymbol{\beta} = (\beta_1, \dots, \beta_N)$. Because we expect the tract-specific parameters to display some spatial continuity, we use priors that explicitly introduce dependence between parameters from neighboring tracts.

Conditionally autoregressive (CAR) models are a popular class of such priors and we use a version introduced in [Leroux et al. \(2000\)](#). Letting $W = (w_{i,j})$ be a binary adjacency matrix with $w_{i,j} = 1$ if and only if neighborhoods i and j share a border, we say that the vector

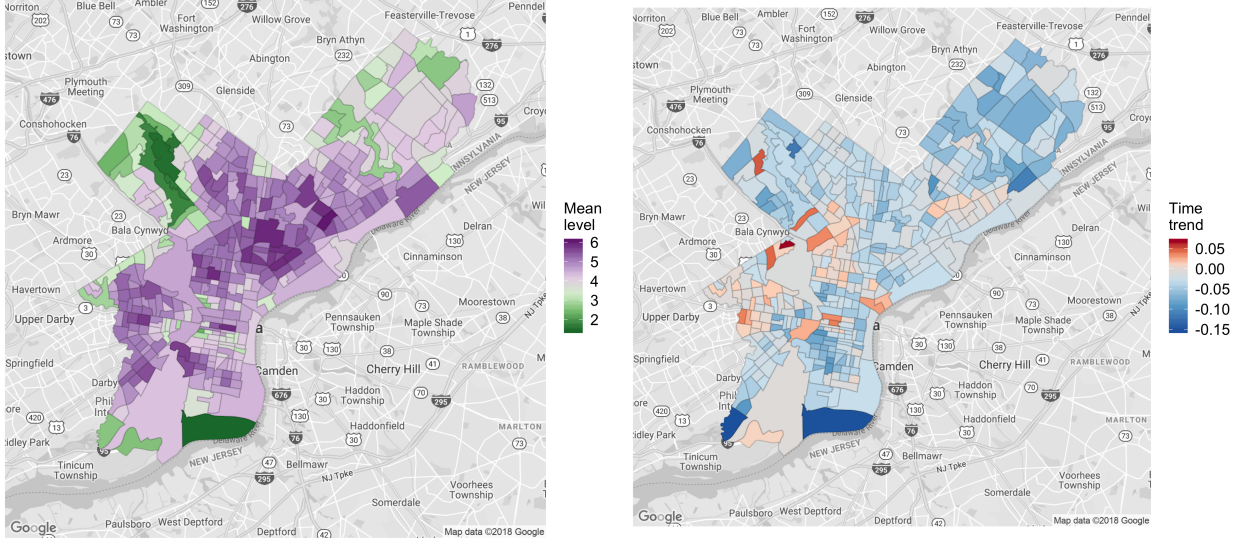


Figure 1: Visualization of the maximum likelihood estimates of the tract-level intercepts α (left panel) and time-trends β (right panel) for the model defined in Section 2.1

$\theta = (\theta_1, \dots, \theta_n)$ follows a CAR model with grand mean $\bar{\theta}$ and variance scale τ^2 if and only if all of the full conditional distributions have the form

$$\theta_i \mid \theta_{-i}, \bar{\theta}, \tau^2 \sim N \left(\frac{(1 - \rho)\bar{\theta} + \rho \sum_j w_{i,j} \theta_j}{1 - \rho + \rho \sum_j w_{i,j}}, \frac{\tau^2}{1 - \rho + \rho \sum_j w_{i,j}} \right).$$

In this CAR model, the conditional mean of $\theta_i \mid \theta_{-i}$ is a weighted average of the grand mean $\bar{\theta}$ and the average of the θ_j 's from the neighborhoods that border neighborhood i . The degree to which θ_i is shrunk toward either of these targets is governed by a parameter ρ , which is typically set by the analyst, and the number of neighbors. These full conditionals uniquely determine the joint distribution $\theta \sim N(\bar{\theta} \mathbf{1}_n, \tau^2 \Sigma_{\text{CAR}})$ where

$$\Sigma_{\text{CAR}} = \begin{cases} [\rho W^* + (1 - \rho)I_n]^{-1} & \text{if } n \geq 2 \\ \frac{1}{1 - \rho} & \text{if } n = 1 \end{cases},$$

$\mathbf{1}_n$ is the n -vector of ones, and W^* is the unweighted graph Laplacian of the adjacency matrix W . For compactness, we will write $\theta \mid \bar{\theta}, \tau^2 \sim \text{CAR}(\bar{\theta}, \tau^2, W)$.

However, cities typically contain many geographic and social barriers like rivers and high-

ways that manifest in sharp spatial discontinuities. In the presence of these discontinuities, a naively specified CAR model can induce a level of spatial smoothness among the parameters at odds with the data. To avoid this behavior, we seek *clusters* of parameters that demonstrate considerable spatial continuity within but not between clusters. We introduce two latent partitions of $[N]$, $\gamma^{(\alpha)}$ and $\gamma^{(\beta)}$, where $\gamma^{(\cdot)} = \{S_1^{(\cdot)}, \dots, S_{K^{(\cdot)}}^{(\cdot)}\}$. We refer to the sets $S_k^{(\cdot)}$ as *clusters* and restrict attention to partitions consisting of clusters of spatially connected neighborhoods. We denote the set of all such partitions by \mathcal{SP} and let $\boldsymbol{\gamma} := (\gamma^{(\alpha)}, \gamma^{(\beta)})$ be the pair of latent spatial partitions underlying the mean level of crime and the time trend of crime across all neighborhoods. In what follows, we will simply refer to $\boldsymbol{\gamma}$ as a *particle*.

To simplify our presentation, we describe only the prior over the mean levels of crime $\boldsymbol{\alpha}$; we place an analogous prior on the time trends $\boldsymbol{\beta}$. We place independent CAR priors on the collections $\boldsymbol{\alpha}_k = \{\alpha_i : i \in S_k^{(\alpha)}\}$, so that the joint prior density $\pi(\boldsymbol{\alpha} \mid \gamma^{(\alpha)}, \sigma^2)$ factorizes over the collection of all clusters: $\pi(\boldsymbol{\alpha} \mid \gamma^{(\alpha)}, \sigma^2) = \prod_{k=1}^{K^{(\alpha)}} \pi(\boldsymbol{\alpha}_k \mid \sigma^2)$. To this end, we introduce a collection of grand cluster means $\bar{\boldsymbol{\alpha}} = \{\bar{\alpha}_1, \dots, \bar{\alpha}_{K^{(\alpha)}}\}$ and model $\boldsymbol{\alpha}_k \mid \bar{\alpha}_k, \sigma^2 \sim \text{CAR}(\bar{\alpha}_k, a_1 \sigma^2, W_k^{(\alpha)})$, where $W_k^{(\alpha)}$ is the sub-matrix of W whose rows and columns are indexed by the cluster $S_k^{(\alpha)}$. We further place independent $N(0, a_2 \sigma^2)$ priors on the grand cluster means $\bar{\alpha}_k$ and place a fully-specific prior Π_γ on $\gamma^{(\alpha)}$. In Sections 4 and 5, we consider two different priors for the latent partitions. The first is a truncated Ewens-Pitman prior with probability mass function

$$\pi(\boldsymbol{\gamma}) \propto \eta^K \prod_{k=1}^K (n_k - 1)! \times \mathbf{1}(\boldsymbol{\gamma} \in \mathcal{SP}). \quad (2)$$

The second is a truncated uniform prior that assigns equal prior probability to each $\boldsymbol{\gamma} \in \mathcal{SP}$. We note here, however, that the computational strategy introduced in Section 3 will work for general priors. We complete our hierarchical prior with an Inverse Gamma prior on the residual variance $\sigma^2 \sim \text{IG}\left(\frac{\nu_\sigma}{2}, \frac{\nu_\sigma \lambda_\sigma}{2}\right)$.

To summarize, our model is

$$\begin{aligned}
\gamma^{(\alpha)}, \gamma^{(\beta)} &\stackrel{iid}{\sim} \Pi_\gamma \\
\sigma^2 &\sim \text{IG}\left(\frac{\nu_\sigma}{2}, \frac{\nu_\sigma \lambda_\sigma}{2}\right) \\
\bar{\alpha}_1, \dots, \bar{\alpha}_{K_\alpha} \mid \gamma^{(\alpha)}, \sigma^2 &\stackrel{iid}{\sim} N(0, a_2 \sigma^2) \\
\bar{\beta}_1, \dots, \bar{\beta}_{K_\beta} \mid \gamma^{(\beta)}, \sigma^2 &\stackrel{iid}{\sim} N(0, b_2 \sigma^2) \\
\boldsymbol{\alpha}_k \mid \bar{\alpha}_k, \sigma^2, \gamma^{(\alpha)} &\sim \text{CAR}(\bar{\alpha}_k, a_1 \sigma^2, W_k^{(\alpha)}) \quad \text{for } k = 1, \dots, K_\alpha \\
\boldsymbol{\beta}_{k'} \mid \bar{\beta}_{k'}, \sigma^2, \gamma^{(\beta)} &\sim \text{CAR}(\bar{\beta}_{k'}, b_1 \sigma^2, W_{k'}^{(\beta)}) \quad \text{for } k' = 1, \dots, K_\beta \\
y_{i,t} \mid \boldsymbol{\alpha}, \boldsymbol{\beta}, \sigma^2 &\sim N(\alpha_i + \beta_i(t - \bar{t}), \sigma^2)
\end{aligned} \tag{3}$$

The high degree of conditional conjugacy in (3) enables us to derive analytic expressions for quantities such as the marginal likelihood $p(\mathbf{y} \mid \boldsymbol{\gamma})$ as well as the conditional posterior expectations $\mathbb{E}[\boldsymbol{\alpha}, \boldsymbol{\beta} \mid \boldsymbol{\gamma}, \mathbf{y}]$. The availability of these expressions will be crucial for the posterior exploration strategy we develop below.

Given the residual variance σ^2 and latent partitions $\gamma^{(\alpha)}$ and $\gamma^{(\beta)}$, parameters in different clusters are conditionally independent. In other words, our model falls with the class of conditional product partition models (PPMs) that have been widely used in Bayesian spatial statistics (see, e.g., [Knorr-Held and Raßer \(2000\)](#), [Denison and Holmes \(2001\)](#), and [Feng et al. \(2016\)](#)). Unlike these papers, however, we are interested in recovering two latent partitions, one each for the mean levels and time-trends within each census tract. In this way, our model is similar to [Anderson et al. \(2017\)](#), who also seek two distinct partitions of the set of neighborhoods. However, unlike [Anderson et al. \(2017\)](#), who limit attention to partitions containing five or fewer clusters for computational simplicity, we do not need to impose any *a priori* restriction on the number of clusters.

3 Posterior Exploration and Summarization

Recall that we have three simultaneous tasks: (i) identify promising particles $\boldsymbol{\gamma} = (\gamma^{(\alpha)}, \gamma^{(\beta)})$, (ii) estimate the mean-levels $\boldsymbol{\alpha}$ and time trends $\boldsymbol{\beta}$ of crime in each neighborhood, and (iii) make predictions about future incidents of crime in each neighborhood. These latter two tasks can generally be expressed as evaluating posterior expectations $\mathbb{E}[f(\boldsymbol{\alpha}, \boldsymbol{\beta}) \mid \mathbf{y}]$ where f

is any functional of interest. The combinatorial vastness of the space \mathcal{SP}^2 , which contains all possible pairs of partitions, renders it impossible to enumerate all particles for even small values of N . As a result, we cannot compute the posterior probability $\pi(\boldsymbol{\gamma} \mid \mathbf{y})$ exactly.

It is tempting to resort to Markov Chain Monte Carlo (MCMC) simulations to approximate expectations $\mathbb{E}[f(\boldsymbol{\alpha}, \boldsymbol{\beta}) \mid \mathbf{y}]$. We could, for instance, proceed in a Gibbs fashion, alternating between updating the two partitions in each $\boldsymbol{\gamma}$ and updating continuous parameters $(\boldsymbol{\alpha}, \boldsymbol{\beta}, \sigma^2)$, while holding the rest fixed. Unfortunately, because we must explore a vast space of pairs of partitions, such MCMC simulations may require a prohibitive amount of time to mix. To get around this difficulty, [Anderson et al. \(2017\)](#) arbitrarily restricted attention to partitions with no more than three to five clusters each. Even with such a restriction, which we will not impose, it is still quite difficult to distill the thousands of resulting draws of $\boldsymbol{\gamma}$ into a single point estimate and to quantify parameter and partition uncertainty.

A popular alternative approach is posterior optimization, which usually focuses on identifying the *maximum a posteriori* (MAP) particle $\hat{\boldsymbol{\gamma}}_{MAP}$ or some other decision-theoretic optimal point estimate (see, e.g., [Lau and Green \(2007\)](#)). One then estimates the marginal expectation $\mathbb{E}[f(\boldsymbol{\alpha}, \boldsymbol{\beta}) \mid \mathbf{y}]$ with a “plug-in” estimator $\mathbb{E}[f(\boldsymbol{\alpha}, \boldsymbol{\beta}) \mid \mathbf{y}, \hat{\boldsymbol{\gamma}}_{MAP}]$. Though this procedure might be substantially faster than MCMC, especially if the marginal likelihood $p(\mathbf{y} \mid \boldsymbol{\gamma})$ possesses certain ordering properties ([Dahl, 2009](#)), it completely eschews exploration of the uncertainty about $\boldsymbol{\gamma}$. As a result, the natural “plug-in” estimator $\mathbb{E}[f(\boldsymbol{\alpha}, \boldsymbol{\beta}) \mid \mathbf{y}, \hat{\boldsymbol{\gamma}}_{MAP}]$ may result in over-confident inference about the function f .

Notice, however, that this plug-in estimator may be viewed as a particular instantiation of Bayesian Model Averaging (BMA) ([Raftery et al., 1997](#); [Hoeting et al., 1999](#)). At a very high-level, BMA aims to approximate the full marginal expectation

$$\mathbb{E}[f(\boldsymbol{\alpha}, \boldsymbol{\beta}) \mid \mathbf{y}] = \sum_{\boldsymbol{\gamma}} \pi(\boldsymbol{\gamma} \mid \mathbf{y}) \mathbb{E}[f(\boldsymbol{\alpha}, \boldsymbol{\beta}) \mid \mathbf{y}, \boldsymbol{\gamma}],$$

by first identifying some small subset Γ of models and then evaluating the more manageable sum

$$f_{\Gamma} = \sum_{\boldsymbol{\gamma} \in \Gamma} \pi_{\Gamma}(\boldsymbol{\gamma} \mid \mathbf{y}) \mathbb{E}[f(\boldsymbol{\alpha}, \boldsymbol{\beta}) \mid \mathbf{y}, \boldsymbol{\gamma}],$$

where π_{Γ} is the restriction of the posterior $\pi(\boldsymbol{\gamma} \mid \mathbf{y})$ to the set Γ .

Intuitively, the better the restricted posterior π_{Γ} approximates the full posterior $\pi(\boldsymbol{\gamma} \mid \mathbf{y})$, the closer f_{Γ} will be to the targeted marginal expectation $\mathbb{E}[f(\boldsymbol{\alpha}, \boldsymbol{\beta}) \mid \mathbf{y}]$. So rather than

just using the top γ , a natural extension of the MAP plug-in is to use the top $L > 1$ γ 's. Specifically if we let $\Gamma_L = \{\gamma^{(1)}, \dots, \gamma^{(L)}\}$ be the L particles with largest posterior mass, we consider

$$f_L = \sum_{\ell=1}^L \tilde{\pi}(\gamma^{(\ell)} | \mathbf{y}) \mathbb{E}[f(\boldsymbol{\alpha}, \boldsymbol{\beta}) | \gamma^{(\ell)}, \mathbf{y}],$$

where $\tilde{\pi}(\cdot | \mathbf{y})$ is the truncation of $\pi(\gamma | \mathbf{y})$ to Γ_L . In contrast to the MAP plug-in estimator, f_L averages over more of the particle selection uncertainty and we might reasonably expect it to be a better approximation of the marginal posterior mean $\mathbb{E}[f(\boldsymbol{\alpha}, \boldsymbol{\beta}) | \mathbf{y}]$. Of course, in order to compute f_L exactly, we know which L particles have the most posterior probability. In the next subsection, we introduce a general strategy for identifying Γ_L based on approximating $\pi(\gamma | \mathbf{y})$ without stochastic search.

3.1 A Variational Approximation

Before proceeding, we introduce a bit more notation. For any collection of L particles $\Gamma = \{\gamma_1, \dots, \gamma_L\}$ and vector $\mathbf{w} = (w_1, \dots, w_L)$ in the L -dimensional simplex, let $q(\cdot | \Gamma, \mathbf{w})$ be the discrete distribution that places probability w_ℓ on the particle γ_ℓ . Following Ročková (2018), we will refer to the collection Γ as a *particle set* and \mathbf{w} as *importance weights*. Let \mathcal{Q}_L be the collection of all such distributions supported on at most L particles. Finally, for each $\lambda > 0$, let Π_λ be the tempered marginal posterior with mass function $\pi_\lambda(\gamma) \propto \pi(\gamma | \mathbf{y})^{\frac{1}{\lambda}}$. Note that the particles in Γ_L , which are the L particles with largest posterior mass, are also the L particles with largest tempered posterior mass for all λ . The following proposition provides the foundation for identifying this collection.

Proposition 1. *Suppose that $\pi(\gamma | \mathbf{y})$ is supported on at least L distinct particles and that $\pi_\lambda(\gamma) \neq \pi_\lambda(\gamma')$ for $\gamma \neq \gamma'$. Let $q_\lambda^*(\cdot | \Gamma^*(\lambda), \mathbf{w}^*(\lambda))$ be the distribution in \mathcal{Q}_L that is closest to Π_λ in a Kullback-Leibler sense:*

$$q_\lambda^* = \arg \min_{q \in \mathcal{Q}_L} \left\{ \sum_{\gamma} q(\gamma) \log \frac{q(\gamma)}{\pi_\lambda(\gamma)} \right\}.$$

Then $\Gamma^(\lambda) = \Gamma_L$ and for each $\ell = 1, \dots, L$, $w_\ell^*(\lambda) \propto \pi(\gamma^{(\ell)} | \mathbf{y})^{\frac{1}{\lambda}}$*

Proof. See Section S1 of the Supplementary Materials. □

In other words, we can find Γ_L by finding an approximation of any tempered posterior Π_λ .

This is equivalent to solving

$$(\Gamma^*(\lambda), \mathbf{w}^*(\lambda)) = \arg \max_{(\Gamma, \mathbf{w})} \left\{ \sum_{\ell=1}^L w_{\ell} \log p(\mathbf{y}, \gamma_{\ell}) + \lambda H(\Gamma, \mathbf{w}) \right\}, \quad (4)$$

where $H(\Gamma, \mathbf{w}) = -\mathbb{E}_q[\log q(\cdot | \Gamma, \mathbf{w})]$ is the entropy of the approximating distribution $q(\cdot | \Gamma, \mathbf{w})$.

Before proceeding, we stress that we are not finding a variational approximation of $\pi(\boldsymbol{\alpha}, \boldsymbol{\beta}, \sigma^2 | \mathbf{y})$, the marginal posterior distribution of the continuous parameters of interest. Instead, we approximate the discrete posterior distribution $\pi(\boldsymbol{\gamma} | \mathbf{y})$, which places positive probability over all particles $\boldsymbol{\gamma} = (\gamma^{\alpha}, \gamma^{\beta})$, with another discrete distribution q^* that places positive probability on only L particles.

We pause briefly to reflect on the two terms in Equation (4). The first term is, up to an additive constant depending only on \mathbf{y} , the \mathbf{w} -weighted average of the height of the log-posterior at each particle in the particle set Γ . This term is clearly maximized when all of the particles in Γ are equal to the MAP. On the other hand, the entropy $H(\Gamma, \mathbf{w})$ of the approximating distribution is maximized when all of the particles in Γ are distinct and each $w_{\ell} = L^{-1}$. The penalty term λ , which we may also view as an inverse temperature, balances these two opposing forces.

3.2 Particle Optimization

Finding the global optimum of (4) exactly is practically impossible, given the enormous size of the set of all possible particle sets Γ . Instead, we deploy a coordinate ascent strategy: starting from an initial particle set Γ and initial weight vector \mathbf{w} , we iteratively update one of \mathbf{w} and Γ until we reach a stationary point.

We initialize the particle set by randomly drawing particles $(\hat{\gamma}_K^{(\alpha)}, \hat{\gamma}_{K'}^{(\beta)})$ with replacement where $\hat{\gamma}_K^{(\alpha)}$ is the partition obtained by running k-means on the maximum likelihood estimates of $\boldsymbol{\alpha}$ with $k = K$ clusters. We let $K, K' = 1, \dots, \lfloor \log(N) \rfloor$. In this initialization, the probability of drawing particle $(\hat{\gamma}_K^{(\alpha)}, \hat{\gamma}_{K'}^{(\beta)})$ is proportional to its marginal posterior probability. Our initialization allows our algorithm to pursue several search directions simultaneously but also allows for some redundancy in the initial particle set. In regions of high posterior probability, such redundancy allows multiple particles to search around a dominant mode, providing a measure of local uncertainty.

Ročková (2018) introduced essentially the same family of optimization problems to identify sparse high-dimensional linear regression models and described a similar coordinate ascent strategy that iteratively updated \mathbf{w} and Γ . In that work, γ was a binary vector indicating which variables to include in the model and the continuous parameters conditional on γ were modeled with continuous spike-and-slab priors in the style of George and McCulloch (1993). To update each individual $\gamma_\ell \in \Gamma$, Ročková (2018) restricted attention only to binary vectors which differed in one coordinate. While it is tempting to update each partition in our setting similarly by re-allocating a single neighborhood to a new or existing cluster, such a strategy is prone to lead to local entrapment.

Indeed, such one-neighborhood updates directly parallel conventional Gibbs samplers for Dirichlet process mixture models (i.e. Algorithms 1 – 8 in Neal (2000)). It is well-known (Celeux et al., 2000) that these samplers can mix very slowly, as their incremental nature make it virtually impossible to pass through regions of low probability between partitions that have similar probability but differ in the cluster assignment of multiple units. In our optimization setting, such a restrictive search strategy results in premature termination at a sub-optimal ensemble Γ . Instead, a more promising strategy for navigating the space of partitions is to allow multiple elements to be re-allocated at once (Jain and Neal, 2004). To this end, we consider both *fine* transitions, which re-allocate a single neighborhood to a new or existing cluster (thereby enabling the creation or removal of “islands”) and *coarse* transitions, which simultaneously re-allocate multiple neighborhoods.

We have two types of coarse transitions, displayed in Figure 2. The first exchanges multiple neighborhoods simultaneously across a border between adjacent clusters, while the second splits an existing cluster into several sub-clusters and merges some or all of the newly created sub-clusters with other existing clusters. We also consider “merge” moves in which two existing adjacent clusters are combined into a single cluster. These merge moves allow for the removal of islands and the reversal of splits. Sometimes, removing a single neighborhood from a cluster leaves the resulting cluster disconnected. When this happens, we treat the resulting components as individual clusters.

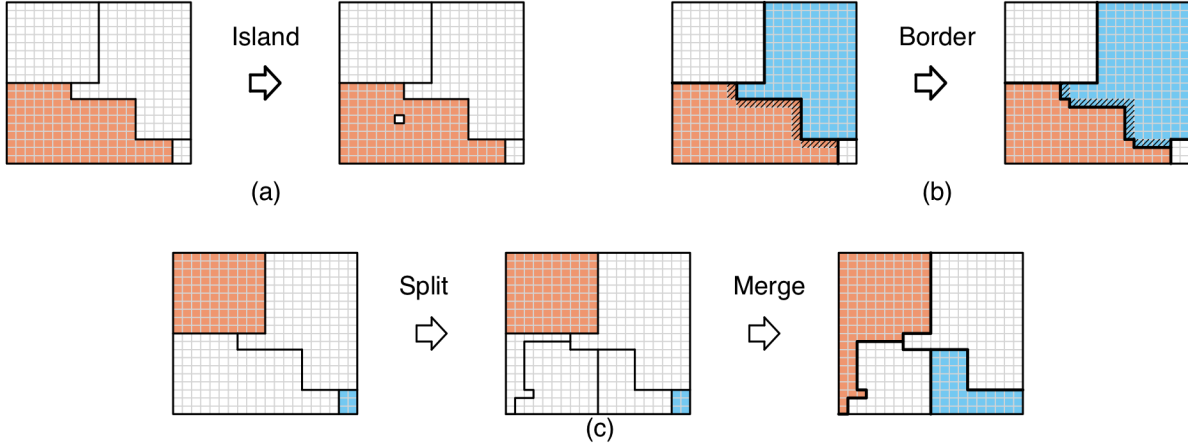


Figure 2: The three broad types of transitions that we consider. An “island” transition (a) removes a single neighborhood from an existing cluster (the lower left orange cluster) and creates a new singleton cluster. A “border” transition moves all neighborhoods at the interface of two adjacent clusters from one cluster to the other. In (b), the neighborhoods moved from the orange cluster to the blue cluster are shaded. The last type of transition (c) first splits an existing cluster (the left cluster in (c)) into multiple parts and then merges some or all of the new sub-clusters into already existing clusters.

In general, we do not attempt all possible coarse and fine transitions while updating a partition. Indeed, there are $O(n)$ possible fine moves and if we allow each of K existing clusters to be split into up to K_{new} sub-clusters, there can be up to $O(K^2 + K \times K_{new}^K)$ possible coarse transitions. Rather than enumerating all of these transitions, we restrict attention to a much smaller set using several heuristics outlined below. For brevity, we describe these heuristics for transitions for $\gamma^{(\alpha)}$; we use exactly the same heuristics for $\gamma^{(\beta)}$.

The conditional conjugacy of our “CAR-within-cluster” model allows us to quickly compute $\mathbb{E}[\alpha_i \mid \gamma, \mathbf{y}]$ and $\mathbb{E}[\bar{\alpha}_k \mid \gamma, \mathbf{y}]$. We use these conditional means as running estimates to propose transitions. For each cluster k , we can identify its nearest neighbor k' , whose estimated grand cluster mean $\bar{\alpha}_{k'}$ is closest to the estimated grand cluster mean of cluster k , $\bar{\alpha}_k$. We then propose exchanging neighborhoods from k across the border between clusters k and k' . In this way, we only consider $O(K)$ coarse transitions of the first type. For coarse moves of the second type, which first split an existing cluster into many pieces, we cap the number of new sub-clusters at $K_{new} = 5$. To generate these sub-clusters, we run both k-means and spectral clustering on the running estimates of the α_i ’s within the cluster. We also propose splits by removing the top or bottom 5% of these estimates.

Once we split a single cluster into many new sub-clusters, we can identify the nearest neighbor of each sub-cluster among the other existing clusters based on the estimated grand cluster means. We then propose a sequence of merges where a new sub-cluster is merged into its nearest neighbor only if all sub-clusters that are closer to their own nearest neighbors are also merged. For fine transitions, we initially only attempt to remove neighborhood i from its current cluster and move it to a new singleton if its estimated α_i is in the top or bottom 5% of the distribution of estimates within the cluster. Following these heuristics, we consider on the order of $N/10$ fine transitions and $O(K + K \times K_{new}^2)$ total coarse transitions while updating a single partition in our ensemble. During our coordinate ascent algorithm, if we find that none of these transitions are accepted, we then try all N fine moves. This last check ensures that our algorithm converges locally in the sense that no one-tract update to an individual partition will result in a higher objective. While these heuristics are somewhat arbitrary, we have found that they work quite well in practice.

4 Synthetic Data Evaluation

To investigate the behavior of our proposed optimization procedure, we consider a simpler model of crime $y_{i,t} = \alpha_i + \sigma \varepsilon_{i,t}$ and we place our CAR-within-cluster prior over α . We simulate data on a 20×20 grid of spatial units partitioned into four clusters of sizes 12, 188, 100, and 100. Figure 3 shows the four clusters in the true partition along with three of the different specifications of α .

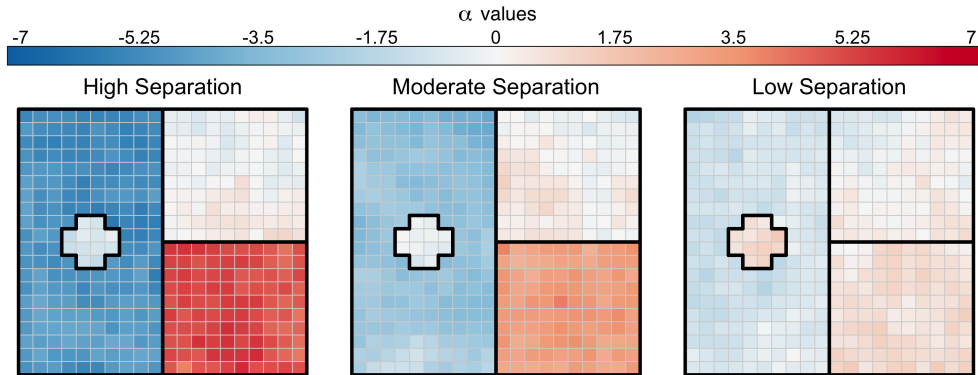


Figure 3: True data generating partition and three different settings of α values. Going from left to right, the distances between the average of the α_i 's within each cluster gets progressively smaller. The color of each square corresponds of the true value of α_i used in the synthetic data generating process.

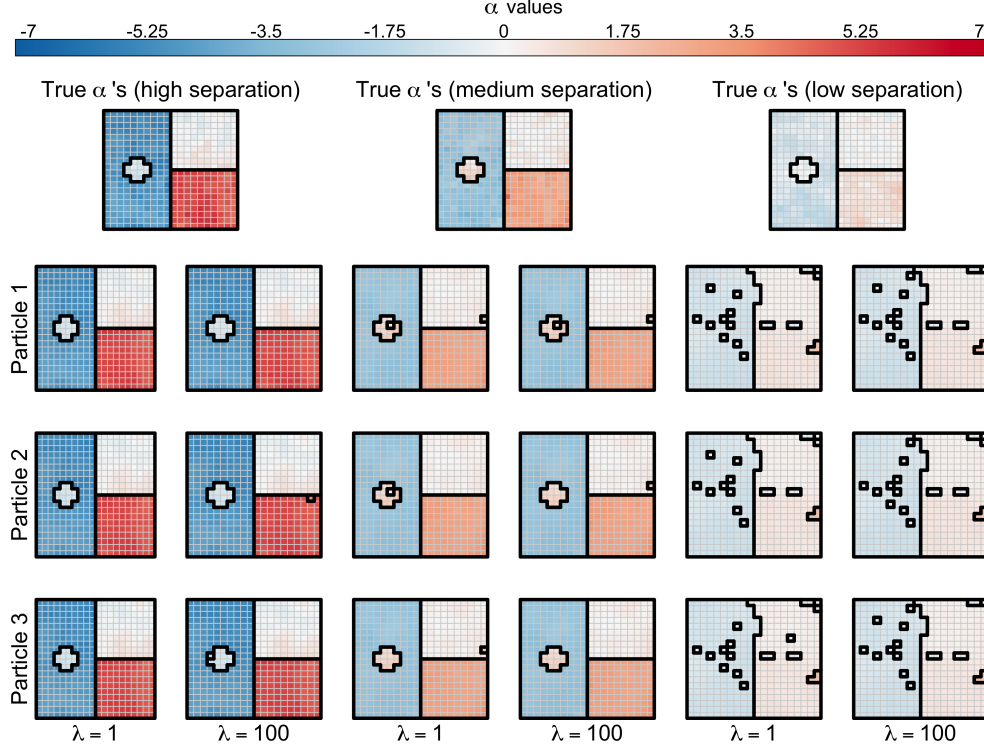


Figure 4: Top three partitions recovered by our particle optimization procedure across different levels of separation of α and values of λ . The color of each square of the recovered particles corresponds to the value of the posterior mean $\mathbb{E}[\alpha_i | \mathbf{y}, \gamma]$. Note, in the high separation setting with $\lambda = 1$, our final particle set contained 10 copies of the same partition.

Figure 4 shows the top three partitions recovered when we run our procedure in each of the high, moderate, and low separation settings with two different entropy penalty parameters $\lambda = 1$ and $\lambda = 100$. We placed a truncated Ewens-Pitman prior (2) on the latent partition with $\eta = 1$. For this demonstration, we fixed $L = 10$, $\rho = 0.9$ and set the remaining hyperparameters according to the heuristics detailed in Section S2 of the Supplementary Materials.

It is reassuring to see that when the clusters are well-separated, our method identifies the true partition as the top particle for both values of λ and that when the clusters are only moderately separated, the top partitions identified are all quite close to the true partition that generated the data. On the other hand, when there is very little separation between the clusters, the partitions returned by our method are visually quite far from the truth. It turns out that these partitions had substantially more posterior probability than the true partition in this setting.

We know from Proposition 1 that the globally optimal particle set Γ_L^* must (i) contain exactly

L particles and (ii) be identical for all values of λ . We see in Figure 4 that in each of the three settings, the top particles identified for $\lambda = 1$ and $\lambda = 100$ are different. In fact, in the high separation setting, all of the particles in our particle set collapsed to the true partition when $\lambda = 1$. Additionally, in the medium separation setting, the second partition identified when $\lambda = 1$ is not contained in the particle set obtained when $\lambda = 100$, despite having more posterior probability than all but the top partition in the latter particle set. This behavior, which is at odds with what might be expected from Proposition 1, highlights the local nature of our optimization algorithm.

Recall that the entropy term in Equation (4) attempts to offset any potential decrease in posterior probability that accompanies a transition away from a high probability particle set already present in the ensemble to a new particle. The fact that the particle set identified in the high separation setting with $\lambda = 1$ displays extreme redundancy – all of the particles collapsed to the same partition – suggests that this entropy term may not always be sufficient to identify L distinct partitions.

This is not altogether surprising: being bounded from above by $\log L$, the changes in entropy encountered by our algorithm are typically orders of magnitude smaller than changes in the \mathbf{w} -weighted (unnormalized) log-posterior. As we increase λ from 1 to 100, however, we find that our procedure recovers $L = 10$ distinct models. In all three settings, we find that some of the particles identified with one choice of λ may not be identified with the other choice of λ , despite having higher posterior probability than many of the particles found with the latter λ . This could also be an artifact of the local, non-reversible, transitions that we consider. Typically, with larger values of λ , particles are encouraged to drift to regions of lower posterior probability more forcefully than with lower values of λ . Moreover, once in those regions, it is typically quite difficult for a particle to “double back” and return to a previously visited state with more posterior probability.

To assess the estimation and partition selection performance of our proposed method quantitatively, we computed the root mean square error (RMSE) of the proposed BMA estimator and the Rand index (Rand, 1971) between the top partition recovered and the true partition averaged over 20 simulated datasets for different choices of cluster separation. The Rand index is defined as the proportion of pairs of elements that are clustered together in both partitions, with values close to one indicating a high degree of similarity between the partitions. Figure 5 shows the average estimation and selection performance for our method run with $\lambda = 1$ along with the following four competitors: (i) the “1-Cluster” model that

places all tracts into a single cluster, (ii) the “N-Clusters” model that places all tracts into singleton clusters, (iii) running k-means on the collection of MLE’s $\hat{\alpha}_i = \bar{y}_{i,\cdot}$, and (iv) running spectral clustering on these tract averages. When running k-means and spectral clustering, we varied the number of clusters from one to ten. For k-means, we selected the number of clusters using the popular elbow method, and for spectral clustering, we found the number of clusters which minimized the total within-cluster sum of squares. We then computed the conditional posterior expectation $\mathbb{E}[\alpha \mid \mathbf{y}, \hat{\gamma}]$ based on the partition $\hat{\gamma}$ estimated from each of the k-means and spectral clustering procedures. Across our simulations, the estimation and partition selection performance of our method with $\lambda = 100$ was virtually identical to the performance with $\lambda = 1$.

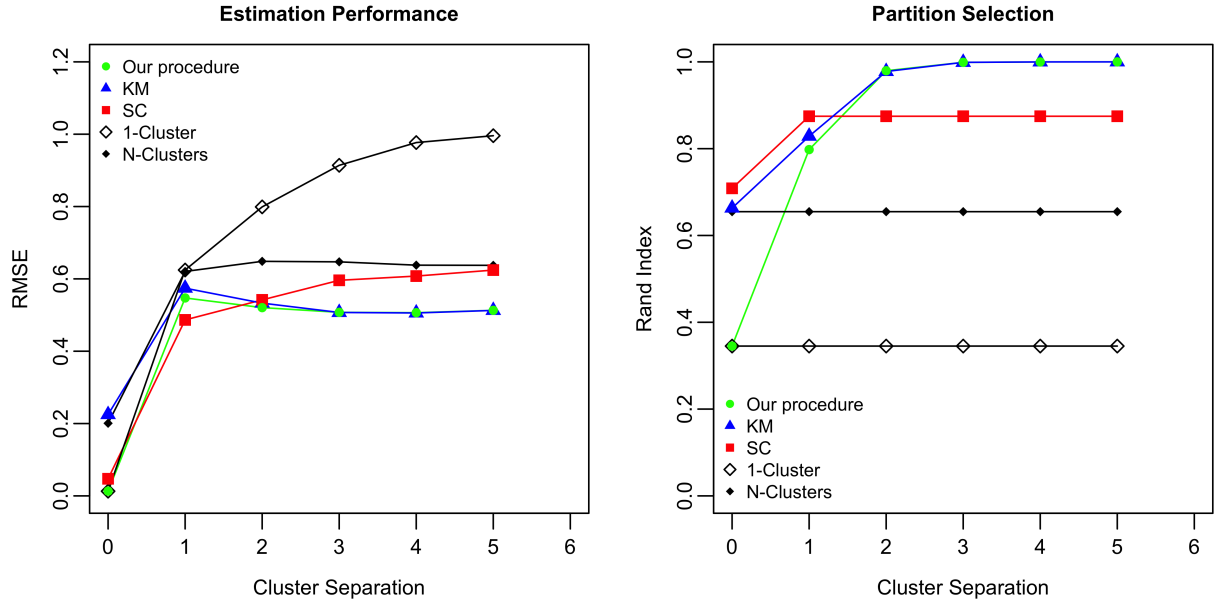


Figure 5: The estimation and partition selection performance, averaged over 20 Monte Carlo simulations, of our method run with $\lambda = 1$ and several competitors across a range of cluster separations.

Immediately we see that, in terms of estimation performance, our procedure is very similar to k-means for non-zero cluster separations. In a certain sense, this behavior is entirely expected when the cluster separation is high: the partition found by k-means in these settings was usually identical to or very close to the true partition, resulting in Rand indices very close to one. However, when the cluster separation is low, our proposed procedure, which identifies several high posterior probability partitions and averages over them, performs much better than k-means, which attempts only to identify a single partition with no reference to the

posterior of interest. When there is in fact no separation between the cluster means, the top partition identified by our procedure was always equal to the partition that placed all tracts in a single cluster. In other words, when there truly was no difference between the cluster means, not only does the trivial “1-Cluster” partition have substantially higher posterior probability than other partitions but our particle optimization strategy is also able to recover this partition reliably. This adaptation, in turn, results in excellent estimation performance in this setting.

Interestingly, our method outperforms spectral clustering, in terms of RMSE, except in one setting where the separation between clusters was low but non-zero. In fact, this was the same low separation setting from Figures 3 and 4. As seen in Figure 4, the partitions identified by our method are all quite different than the true partition. It turns out that in this setting, the partition identified by spectral clustering divided the tracts into four equally sized 10×10 grids; see Figure S1 in Section S3 of the Supplementary Materials. This partition is substantially closer to the true partition and it is therefore perhaps not surprising that spectral clustering achieved slightly better RMSE in this setting.

In Figure 5, we showed the RMSE for the full BMA estimator that averaged over all of the particles recovered by our method. Especially when the separation between clusters was very large, often the top partition identified had orders of magnitude more posterior probability than the other partitions identified. This raises a natural question: could we achieve somewhat better estimation performance by averaging over only a subset of the partitions identified by our method instead of averaging over all of them? In our experiments, we found that it was usually better to average over multiple partitions instead of focusing on the MAP plug-in. However, the RMSE was not monotonic in the number of particles averaged over. We also found that the change in RMSE as we varied the number of particles averaged over was quite small, typically of order 10^{-4} or less.

5 Clustering Crime Dynamics in Philadelphia

As described in Section 2, we model the transformed number of violent crimes $y_{i,t}$ in neighborhood i at time t as $y_{i,t} = \alpha_i + \beta_i(t - \bar{t}) + \varepsilon_{i,t}$. We further wish to identify two partitions of neighborhoods: one, $\gamma^{(\alpha)}$, that clusters together neighborhoods with similar mean levels of crime α_i , and the other, $\gamma^{(\beta)}$, that clusters together neighborhoods with similar time trends β_i .

For our analysis of the Philadelphia crime data, we consider two priors on the partitions $\gamma^{(\alpha)}$ and $\gamma^{(\beta)}$: the Ewen-Pitman prior (2) with hyper-parameter $\eta = 5$ and the uniform prior, both of which are truncated to the set of spatially connected partitions \mathcal{SP} . In this analysis, we set $L = 10$, $\lambda = 100$ and set the remaining hyper-parameters using the heuristics described in Section S2 of the Supplementary Materials. The top panel of Figure 6 shows the top three particles recovered when we placed independent Ewens-Pitman priors on each of $\gamma^{(\alpha)}$ and $\gamma^{(\beta)}$ while the bottom panel of the figure displays the top three particles recovered with uniform priors on the latent partitions. In Figure 6 we display the top particles as colored maps in which thick lines depict borders between clusters and the color of each neighborhood corresponds to the conditional mean of the α_i 's or β_i 's given the partitions $\gamma^{(\alpha)}$ and $\gamma^{(\beta)}$. To illustrate the differences between the identified partitions, we have added grayscale “difference plots” between the colored plots that shade the neighborhoods that are clustered differently. When two partitions are equal, no neighborhoods are shaded in the difference plot.

Similar to our synthetic experiments in Figure 4, some of the identified partitions differ only in the cluster assignment of a small number of neighborhoods. For instance, when we placed a Ewens-Pitman prior on the time-trend partition $\gamma^{(\beta)}$, the top two particles differ in their assignment of a single neighborhood in Northeast Philadelphia. As seen in the second row of Figure 6, while the top particle isolates this neighborhood (labelled A in the figure) in a singleton cluster with a strongly decreasing time trend (ie. large negative β_i estimate), the second particle places this neighborhood in a larger cluster with only a moderately decreasing time trend.

Unlike our synthetic experiments, however, some of the identified partitions of the real data differ substantially. This is especially pronounced in the time trend partitions identified when we placed a uniform prior on $\gamma^{(\beta)}$ (bottom row of Figure 6). The first and third particles, for instance, differ substantially in their clustering of neighborhoods in South and West Philadelphia. This difference is most apparent in the large neighborhood (labelled B in the figure) containing the southern sections of the Schuylkill river: the first particle estimates a moderately increasing time trend in this neighborhood and separates it from the neighborhoods immediately to its east and west that have decreasing time trends. In contrast, the third particle clusters all of these neighborhoods together and estimates a decreasing time trend in all of them.

Figure 6 also reveals the sensitivity of the posterior over the partitions to the choice of priors.

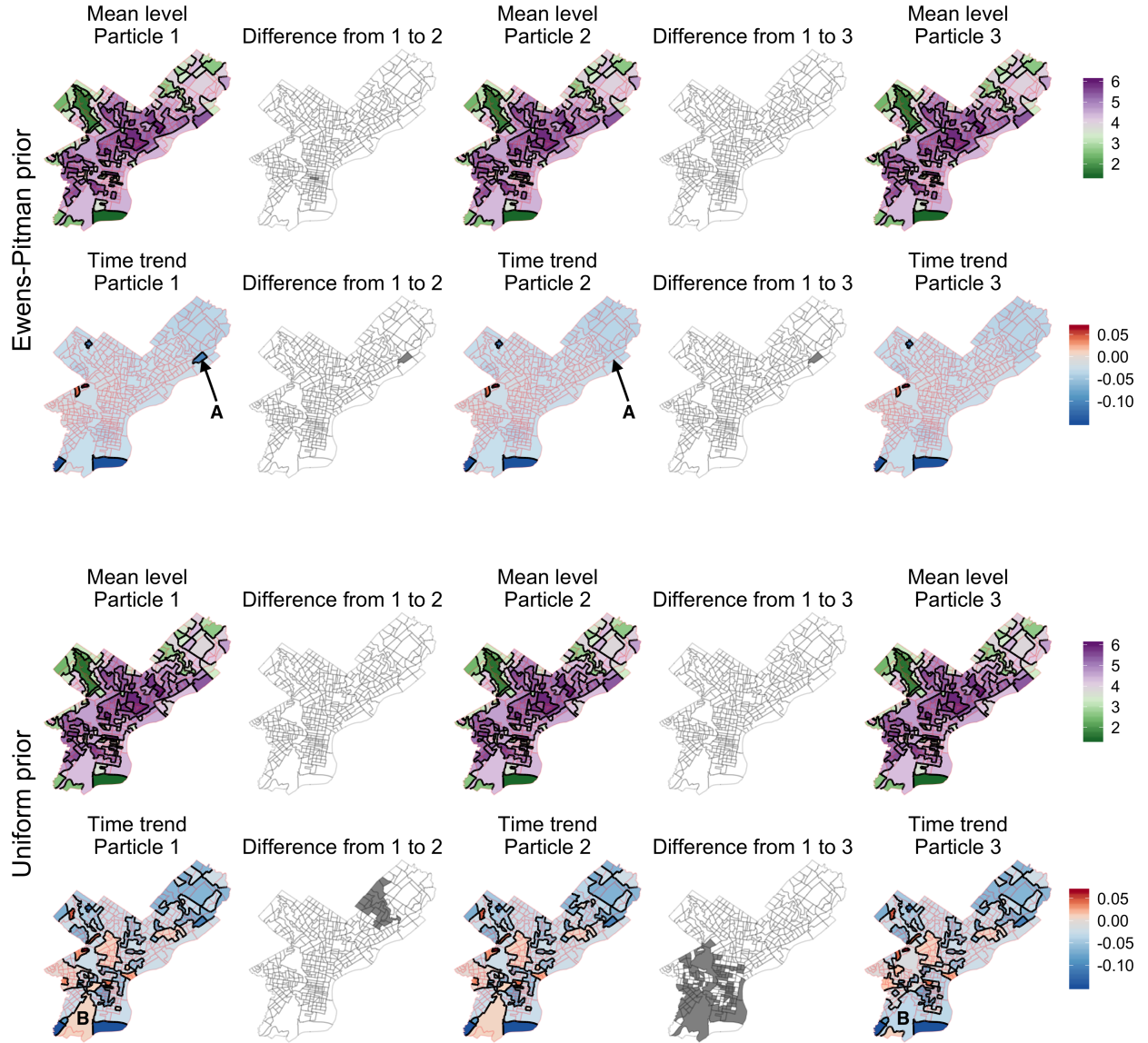


Figure 6: Colored plots: Top three particles identified by our procedure. The thick borders represent the partition, and the color represents the posterior mean of the parameters α and β . Black and white plots: difference plots showing in gray the areas where the cluster assignments change between two partitions. **Top:** Ewens-Pitman prior with $\eta = 5$. **Bottom:** Uniform prior on SP .

Specifically, we recover many more clusters when we placed uniform priors on the partitions than when we placed Ewens-Pitman priors. We see this contrast best in the recovered time trend partitions $\gamma^{(\beta)}$. As we see in the second row of Figure 6, with the Ewens-Pitman prior, we recover a relatively small number of clusters: one very large cluster that contains nearly all neighborhoods with an estimated mildly decreasing time trend and a handful of singleton clusters that display more extreme increasing or decreasing time trends. In contrast, with the uniform prior (fourth row of Figure 6), we recover many more clusters. Like with the Ewens-Pitman prior, we still identify some singleton clusters corresponding to more extreme time trends but also identify many moderately sized clusters that display a range of time trends, both increasing and decreasing. Interestingly, though we recover more clusters in the mean level partition $\gamma^{(\alpha)}$ with a uniform prior, the estimates of α_i arising from both priors show little substantive difference.

While Figure 6 compares the top three identified particles, Figure 7 visualizes the overall variation in the entire particle set. Moreover while the former depicts both the parameter estimates in the colored plots and the partition differences in the grayscale plots, the latter only focuses on representing the partition differences. We first depict the top particle and represent the cluster borders with thick lines and then we shade each neighborhood that is assigned to a different cluster in any of the remaining particles $\gamma_{(\ell)}$ for $\ell = 2, \dots, L$. In this way, we may regard the plots in Figure 7 as the superimposition of the grayscale difference plots computed for each pair $(\gamma_{(1)}, \gamma_{(\ell)})$. The left panel of Figure 7 displays the difference in the partitions of the average level of crime $\gamma^{(\alpha)}$ recovered under the Ewens-Pitman prior. From this plot, we see immediately that all of the recovered mean level partitions differ in their cluster assignment of only a small number of neighborhoods. The right panel displays a similar representation of the recovered time trend partitions $\gamma^{(\beta)}$ under a uniform prior. We see that there is much more variability in the cluster assignment across the particles, with most of the differences concentrated in South and West Philadelphia. It is not entirely surprising that there is less variability among the partitions recovered using a Ewens-Pitman prior than among partitions recovered with a uniform prior. Essentially, in our local search algorithm, the uniform prior will always favor splitting a large cluster into smaller clusters, even if the corresponding change in marginal likelihood is small. This allows the algorithm to discover very different partitions with similarly large posterior probabilities. In contrast, the Ewens-Pitman prior tends to favor fine transitions like island moves over coarser moves that simultaneously re-allocate multiple neighborhoods. As a result, the discovered partitions tend to be quite similar to one another under the Ewens-Pitman prior.

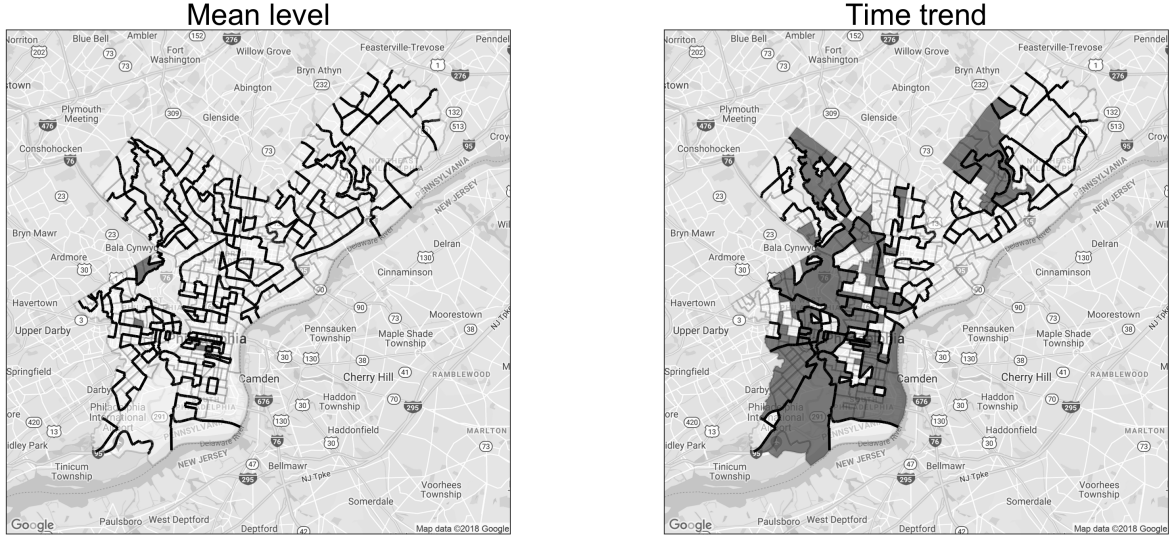


Figure 7: Visualization of the overall partition variation in the particle set. The thick black lines depict the top partition and the shaded areas highlight the neighborhoods that had a different cluster assignment in at least one of the other nine particles. Left panel: variation in $\gamma^{(\alpha)}$ when using the Ewens-Pitman prior. Right panel: variation in $\gamma^{(\beta)}$ when using the uniform prior on \mathcal{SP} .

Having identified several plausible partitions of the neighborhoods, we now assess the predictive accuracy of our crime model. In addition to the two prior specifications considered in Figure 6, we consider two “hybrid” priors: one in which we place a Ewens-Pitman prior on $\gamma^{(\alpha)}$ and a uniform prior on $\gamma^{(\beta)}$ and the other in which we place a uniform prior on $\gamma^{(\alpha)}$ and a Ewens-Pitman prior on $\gamma^{(\beta)}$. Figure S2 in the Supplementary Materials is an analog of Figure 6 that depicts the top three particles identified using these two hybrid priors.

Table 1 reports the out-of-sample RMSE for predicting the level of crime in each neighborhood in 2018 for each of the four different partition prior specifications. The column labelled “Top Particle” reports the RMSE of predictions made using the estimates of α and β from only the top particle (i.e. the MAP estimate of γ) while the column labelled “BMA” reports the predictions made by averaging over all of the identified particles with BMA. We compare the predictive performance of our method under these four prior specifications to a method that does not impose any shrinkage or clustering and instead makes predictions based only on the maximum likelihood estimates of α and β .

Table 1: Out-of-sample RMSE using different combinations of priors for the partitions $\gamma^{(\alpha)}$ and $\gamma^{(\beta)}$. The row labelled MLE corresponds to the method which predicts crime in 2018 using the MLE of α and β computed using data from 2006 – 2018. The next four rows correspond to the different specifications of the priors on partitions with the prior on $\gamma^{(\alpha)}$ listed first.

	Top particle	BMA
MLE	0.2340	-
EP-EP prior	0.2568	0.2560
Uniform-Uniform prior	0.2327	0.2325
EP-Uniform prior	0.2339	0.2319
Uniform-EP prior	0.2546	0.2539

We see that using a uniform prior on $\gamma^{(\beta)}$ yielded better predictive performance than using a Ewens-Pitman prior. As we see in the second row of Figure 6 and the fourth row of Figure S2, with a Ewens-Pitman prior, the vast majority of estimated β_i 's are negative, indicative of overall average decreasing time trend across the entire city. With a uniform prior (fourth row of Figure 6 and second row of Figure S2), we instead recover a more nuanced picture: while the overall average time trend across the entire city may be negative, there are pockets of increasing time trends throughout the city. In a certain sense, because the Ewens-Pitman prior strongly discourages the formation of a large number of clusters and instead clusters most of the neighborhoods together, it leads to incorrect estimation of the *sign* of several β_i 's. Within our simple linear model, incorrect sign estimation can substantially bias future crime forecasts.

In Table 1, we see that placing a Ewens-Pitman prior on $\gamma^{(\alpha)}$ and a uniform prior on $\gamma^{(\beta)}$ yielded the best predictive performance. Figure 8 depicts the top particle identified under this prior specification.

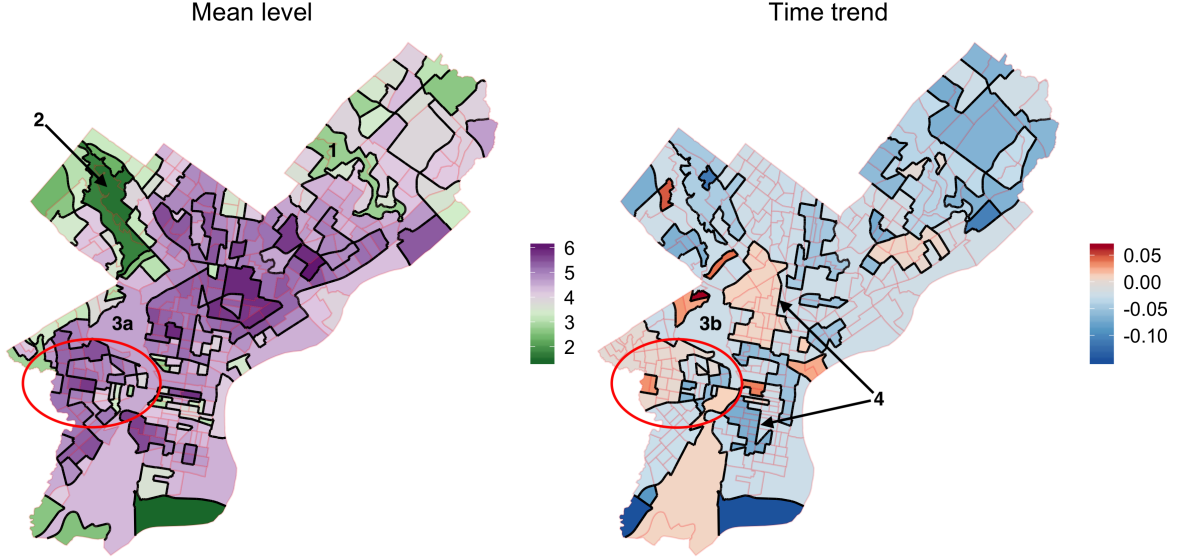


Figure 8: Partitions (thick black lines) and posterior mean coefficients (colors) in the top particle under the EP prior on $\gamma^{(\alpha)}$ and uniform prior on $\gamma^{(\beta)}$, which is the model with the smallest prediction error (in the BMA sense).

We recognize many aspects of Philadelphia’s geography directly from the cluster structure shown in Figure 8. For instance, the clusters labelled **1** and **2** in the figure correspond to the areas surrounding the Pennypack and Wissahickon rivers, respectively. Further, several cluster borders coincide exactly with the boundaries of Fairmount Park (indicated by **3a** and **3b** in the figure) and the major arterial road Broad Street (labelled **4**).

We finally analyze the West Philadelphia and University City region (circled in Figure 8), which contains both Drexel University and the University of Pennsylvania. For the most part, this region is characterized by relatively high levels of crime (darker shades of purple in the left panel of the figure) with the exception of two neighborhoods that are immediately adjacent to the universities (lighter green shades). There is substantial heterogeneity in the estimated time trend within the region as well. Notably, we estimate a decreasing trend in the neighborhoods in the immediate vicinity of the universities and a slightly increasing trend further away from the universities. This finding aligns with previous reports of the positive impact of the University of Pennsylvania’s West Philadelphia Initiatives aimed at improving the social and economic landscape around the university campus (Ehlenz, 2016).

6 Discussion

Accurate estimation of the change in crime over time is a critical first step towards a better understanding of public safety in large urban environments. An especially important challenge to such estimation is the potential presence of sharp discontinuities, which may be smoothed over by naive spatial shrinkage procedures. Focusing on the city of Philadelphia, we introduced a Bayesian hierarchical model that naturally identifies these discontinuities by partitioning the city into several clusters of neighborhoods and introduces spatial smoothness within but not between clusters. In particular, we focused on recovering two latent spatial partitions, one for the mean-level of crime over the twelve year period 2006 – 2017 and one for the time-trend.

Rather than use a computationally prohibitive stochastic search, we instead sought to identify partitions with highest posterior probability by solving a single optimization problem. We showed that optimizing the proposed objective function is formally equivalent to finding a particular variational objective and introduced a local search strategy for solving this problem. While our primary focus has been on crime in the city of Philadelphia, our ensemble optimization framework is more general and there are a number of areas of future development, which we discuss below.

The results of our applied analysis were quite sensitive to the choice of prior placed on the underlying spatial partition. With a Ewens-Pitman prior, nearly all of the neighborhood time trends were assigned to a single cluster while with a uniform prior, we obtained a much richer cluster structure. It would be interesting to construct an objective prior for spatial partitions along the lines of [Casella et al. \(2004\)](#).

While it may be sufficient to consider a linear temporal model of crime when there are relatively few time points ([Bernardinelli et al., 1995](#); [Anderson et al., 2017](#)), with more observations per census tract, it is reasonable to consider more flexible models. For instance, we could model $y_{i,t} \sim N(f_i(\mathbf{x}_{i,t}), \sigma^2)$ and place Gaussian process priors over the f_i 's within each cluster. Such an elaboration retains conditional conjugacy and we can still use our ensemble optimization strategy to identify clusters with high posterior probability, though computing the marginal likelihood $p(\mathbf{y} \mid \boldsymbol{\gamma})$ is somewhat more involved. It is more difficult to deploy our ensemble optimization strategy directly when the marginal likelihood $p(\mathbf{y} \mid \boldsymbol{\gamma})$ is not available in closed-form. While it may sometimes be possible to use an EM algorithm like [Ročková \(2018\)](#), this is not always feasible for more complicated models. One very natural

idea would be to estimate the marginal likelihood with a Laplace approximation.

In many of our empirical examples and especially when we used Ewens-Pitman priors, the particle set can remain stuck in the vicinity of a dominant mode. When this happens, it is not immediately obvious whether the posterior truly concentrates around a single dominant mode or if there are other pockets of substantial posterior mass that are far away. Unfortunately, the entropy term in Equation 4 may provide insufficient repulsion between the particles to probe this latter possibility. Operationally, the entropy term discourages redundancy in the particle set by penalizing exact equality between particles but does not penalize placing a particle in the vicinity of another model that is already present in the particle set. One way around this potential weakness is to augment the optimization objective in (4) with an additional penalty term that directly penalizes the pairwise distance between particles in the particle set. In doing so, however, we would lose the guarantee of optimality afforded by Proposition 1.

References

- Anderson, C., Lee, D., and Dean, N. (2017). Spatial clustering of average risks and risk trends in bayesian disease mapping. *Biometrical Journal*, 59(1):41–56.
- Balocchi, C. and Jensen, S. T. (2019). Spatial modeling of trends in crime over time in Philadelphia. *Annals of Applied Statistics*, 13(4):2235–2259.
- Banerjee, S., Carlin, B. P., Li, P., and McBean, A. M. (2012). Bayesian areal wombling using false discovery rates. *Statistics and its Interface*, 5(2):149–158.
- Bernardinelli, L., Clayton, D., Pascutto, C., Montomoli, C., Ghislandi, M., and Songini, M. (1995). Bayesian analysis of space—time variation in disease risk. *Statistics in medicine*, 14(21-22):2433–2443.
- Besag, J. (1974). Spatial interaction and the statistical analysis of lattice systems. *Journal of the Royal Statistical Society. Series B (Methodological)*, pages 192–236.
- Boots, B. (2001). Using local statistics for boundary characterization. *GeoJournal*, 53(4):339–345.

- Burbidge, J. B., Magee, L., and Robb, A. L. (1988). Alternative transformations to handle extreme values of the dependent variable. *Journal of the American Statistical Association*, 83(401):123–127.
- Casella, G., Moreno, E., and Girón, F. J. (2004). Cluster analysis, model selection, and prior distributions on models. *Bayesian Analysis*, 9(3):613 – 685.
- Celeux, G., Hurn, M., and Robert, C. P. (2000). Computational and inferential difficulties with mixture posterior distributions. *Journal of the American Statistical Association*, 95(451):957 – 970.
- Dahl, D. B. (2009). Modal clustering in a class of product partition models. *Bayesian Analysis*, 4(2):243 – 264.
- Denison, D. and Holmes, C. (2001). Bayesian partitioning for estimating disease risk. *Biometrics*, 57(1):143–149.
- Ehlenz, M. M. (2016). Neighborhood revitalization and the anchor institution: Assessing the impact of the university of pennsylvania’s west philadelphia initiatives on university city. *Urban Affairs Review*, 52(5):714 – 750.
- FBI (2011). Uniform Crime Reporting program, definitions. <https://ucr.fbi.gov/crime-in-the-u.s/2011/crime-in-the-u.s.-2011/offense-definitions>. Accessed: 2016-09-15.
- Feng, W., Lim, C. Y., Maiti, T., and Zhang, Z. (2016). Spatial regression and estimation of disease risks: A clustering-based approach. *Statistical Analysis and Data Mining: The ASA Data Science Journal*, 9(6):417–434.
- George, E. I. and McCulloch, R. E. (1993). Variable selection via Gibbs sampling. *Journal of the American Statistical Association*, 88(423):881 – 889.
- Hoeting, J. A., Madigan, D., Raferty, A. E., and Volinsky, C. T. (1999). Bayesian model averaging: a tutorial. *Statistical Science*, 14(4):382 – 417.
- Jain, S. and Neal, R. (2004). A split-merge Markov chain Monte Carlo procedure for the Dirichlet Process mixture model. *Journal of Computational and Graphical Statistics*, 13(1):158 – 182.

- Knorr-Held, L. and Raßer, G. (2000). Bayesian detection of clusters and discontinuities in disease maps. *Biometrics*, 56(1):13–21.
- Lau, J. W. and Green, P. J. (2007). Bayesian model-based clustering procedures. *Journal of Computational and Graphical Statistics*, 16(3):526–558.
- Lee, D. and Mitchell, R. (2012). Boundary detection in disease mapping studies. *Biostatistics*, 13(3):415–426.
- Lee, D. and Mitchell, R. (2013). Locally adaptive spatial smoothing using conditional autoregressive models. *Journal of the Royal Statistical Society: Series C (Applied Statistics)*, 62(4):593–608.
- Leroux, B. G., Lei, X., and Breslow, N. (2000). Estimation of disease rates in small areas: a new mixed model for spatial dependence. In *Statistical models in epidemiology, the environment, and clinical trials*, pages 179–191. Springer.
- Li, P., Banerjee, S., and McBean, A. M. (2011). Mining boundary effects in areally referenced spatial data using the bayesian information criterion. *Geoinformatica*, 15(3):435–454.
- Lu, H. and Carlin, B. P. (2005). Bayesian areal wombling for geographical boundary analysis. *Geographical Analysis*, 37(3):265–285.
- Lu, H., Reilly, C. S., Banerjee, S., and Carlin, B. P. (2007). Bayesian areal wombling via adjacency modeling. *Environmental and Ecological Statistics*, 14(4):433–452.
- Neal, R. (2000). Markov Chain sampling methods for Dirichlet Process mixture models. *Journal of Computational and Graphical Statistics*, 9(2):249 – 265.
- Raftery, A. E., Madigan, D., and Hoeting, J. A. (1997). Bayesian model averaging for linear regression models. *Journal of the American Statistical Association*, 92(437):179 – 191.
- Rand, W. M. (1971). Objective criteria for the evaluation of clustering methods. *Journal of the American Statistical association*, 66(336):846–850.
- Ročková, V. (2018). Particle EM for variable selection. *Journal of the American Statistical Association*, 113(524):1684 – 1697.

Supplementary Materials for

“Crime in Philadelphia: Bayesian Clustering with Particle Optimization”

1 Proof of Proposition 1

In this Section 3.1 we state that we can find the set of L particles with largest posterior by finding a variational approximation of the tempered posterior Π_λ . Here we restate Proposition 1 and provide the proof.

Remember that we denote with $\Gamma_L = \{\gamma^{(1)}, \dots, \gamma^{(L)}\}$ the set of L particles with largest posterior mass, with $q(\cdot \mid \Gamma, \mathbf{w})$ the discrete distribution that places probability w_ℓ on the particle γ_ℓ and with \mathcal{Q}_L the collection of all such distributions supported on at most L particles. Moreover, for each $\lambda > 0$, let π_λ be the mass function of the tempered marginal posterior Π_λ , where $\pi_\lambda(\gamma) \propto \pi(\gamma \mid \mathbf{y})^{\frac{1}{\lambda}}$.

Proposition 1. *Suppose that $\pi(\gamma \mid \mathbf{y})$ is supported on at least L distinct particles and that $\pi_\lambda(\gamma) \neq \pi_\lambda(\gamma')$ for $\gamma \neq \gamma'$. Let $q_\lambda^*(\cdot \mid \Gamma^*(\lambda), \mathbf{w}^*(\lambda))$ be the distribution in \mathcal{Q}_L that is closest to Π_λ in a Kullback-Leibler sense:*

$$q_\lambda^* = \arg \min_{q \in \mathcal{Q}_L} \left\{ \sum_{\gamma} q(\gamma) \log \frac{q(\gamma)}{\pi_\lambda(\gamma)} \right\}.$$

Then $\Gamma^(\lambda) = \Gamma_L$ and for each $\ell = 1, \dots, L$, $w_\ell^*(\lambda) \propto \pi(\gamma^{(\ell)} \mid \mathbf{y})^{\frac{1}{\lambda}}$*

Proof. Denote the optimal particles $\Gamma^*(\lambda) = \{\gamma_1^*, \dots, \gamma_{L^*}^*\}$. Straightforward calculus verifies that $w_\ell^*(\lambda) \propto \pi_\lambda(\gamma_\ell^*)$. We thus compute

$$\text{KL}(q^* \parallel \pi_\lambda) = \sum_{\gamma} q^*(\gamma) \log \frac{q^*(\gamma)}{\pi_\lambda(\gamma)} = -\log \Pi_\lambda(\Gamma^*(\lambda))$$

Since Π_λ is supported on at least L models, we see from this computation that if Γ^* contained fewer than L particles, we could achieve a lower Kullback-Leibler divergence by adding another particle $\tilde{\gamma}$ not currently in Γ^* that has positive Π_λ -probability to the particle set and updating the importance weights \mathbf{w} accordingly.

Now if Γ^* contains L models but $\Gamma^*(\lambda) \neq \Gamma_L$, we know $\Pi_\lambda(\Gamma^*(\lambda)) < \Pi_\lambda(\Gamma_L)$. Thus, replacing $\Gamma^*(\lambda)$ by Γ_L and adjusting the importances weights accordingly would also result in a lower Kullback-Liebler divergence. \square

2 Various hyper-parameter choices

The main model described in Section 2 depends on several hyper-parameters, which need to be fixed by the practitioner: the parameters for the prior for σ (ν_σ and λ_σ) and the multiplicative constants to specify within and between cluster variance (a_1, a_2, b_1 and b_2). We will now describe the heuristic used to specify such values.

Let us consider each neighborhood separately and fit a simple linear regression model in each one: let $\hat{\alpha}_i$ and $\hat{\beta}_i$ be the least square estimates and $\hat{\sigma}_i^2$ be the estimated residual variance for neighborhood i . Since these estimates do not incorporate any prior information or sharing of information, we can think of them as an approximation of α_i, β_i given the partition with N clusters γ_N ; in fact under such configuration the coefficients are exchangeable and the only shrinkage induced is through the common variance parameter. Given this, one heuristic desideratum is that the marginal prior on $\alpha \mid \gamma = \gamma_N$ should assign substantial probability to range of the $\hat{\alpha}_i$. Specifically, we will make sure that this conditional prior places 95% of its probability over the range of the $\hat{\alpha}_i$'s. Since $\alpha \mid \gamma = \gamma_N \sim N(0, \sigma^2(a_1/(1 - \rho) + a_2)I_n)$, we constrain a_1 and a_2 so that

$$\frac{a_1}{1 - \rho} + a_2 = \frac{\max_i |\hat{\alpha}_i|^2}{4\hat{\sigma}^2}.$$

In order to determine each of a_1 and a_2 , we need a second constraint. To this end, consider the highly stylized setting in which we have K overlapping clusters with equal variance σ_{cl}^2 whose means are equally spaced at distance $2\sigma_{cl}$. The idea of this second heuristic is to match such a stylized description to the observe distribution of $\hat{\alpha}_i$. In essence, this involves covering the range of $\hat{\alpha}_i$ with $K + 1$ “chunks” of length $2\sigma_{cl}$. While the exact value of σ_{cl} is unknown, we have found it useful to approximate it $a_1\sigma^2/(1 - \rho)$. This approximation tends to produce smaller values of a_1 , which in turn encourages a relatively small number of clusters.

With these two constraints we find:

$$a_1 = \frac{(\max(\hat{\alpha}_i) - \min(\hat{\alpha}_i))^2}{4(K+1)^2\hat{\sigma}^2/(1-\rho)}$$

$$a_2 = \frac{\max_i |\hat{\alpha}_i|^2}{4\hat{\sigma}^2} - \frac{a_1}{1-\rho}.$$

Similarly for the $\hat{\beta}_i$'s we find:

$$b_1 = \frac{(\max(\hat{\beta}_i) - \min(\hat{\beta}_i))^2}{4(K+1)^2\hat{\sigma}^2/(1-\rho)}$$

$$b_2 = \frac{\max_i |\hat{\beta}_i|^2}{4\hat{\sigma}^2} - \frac{b_1}{1-\rho}.$$

In order to operationalize these heuristics, we must specify an initial guess at K . We have found in our experiments, setting $K = \lfloor \log N \rfloor$ works quite well. It, moreover, accords with the general behavior of the Ewens-Pitman prior.

Finally, to specify the prior for σ^2 we can use the collection of $\hat{\sigma}_i^2$'s: by matching mean and variance, we can recover $\nu_\sigma = 2\frac{m^2}{v} + 4$ and $\lambda_\sigma = m(1 - \frac{2}{\nu_\sigma})$, where m and v are the empirical mean and variance of the $\hat{\sigma}_i^2$'s.

3 Additional Synthetic Data Evaluation

In Section 4, we generated several synthetic datasets based on a 20 grid of census tracts partitioned into four clusters of size 12, 188, 100, and 100, as seen in Figure 3. Within each cluster, we drew the α_i 's from a CAR model centered at a specified cluster mean with $\rho = 0.95$ and variance scale 0.2. Across the different specifications of cluster means, we always fixed the cluster mean of the 12-tract ‘‘cross’’ and the 100 tract square in the upper right corner to be zero. We then fixed the mean of the 188-tract cluster on the left hand side to be $-\Delta$ and the mean of the 100-tract cluster in the lower right corner to be Δ . We generated datasets for each of $\Delta = 0, 1, \dots, 5$. The high, medium, and low separation settings in Figure 3 and 4 correspond to $\Delta = 5, 3$, and 1, respectively.

In Section 4, we compared the partition selection performance of our method to that of k-means and spectral clustering. Figure S1 shows the estimated partitions from k-means and

spectral clustering on the same dataset used to generate Figure 4. Across these datasets, the optimal number of clusters for k-means was always three, according to the “elbow method.” However, because k-means does not implicitly account for our spatial connectedness constraints, we post-processed the recovered partition by treating disconnected parts of clusters identified by k-means as their own separate clusters.

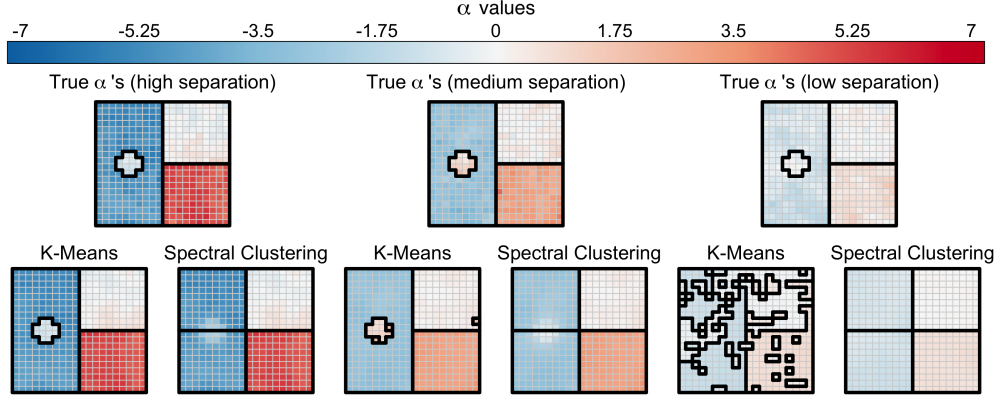


Figure S1: Partitions recovered by k-means and spectral clustering for three different cluster separation settings. The color of each tract corresponds to the estimated parameter value $\mathbb{E}[\alpha_i \mid \mathbf{y}, \boldsymbol{\gamma}]$.

4 Additional Results for Clustering in Philadelphia

In figure S2 we represent the best three particles recovered by the models where the priors are specified as Ewens-Pitman prior with $\eta = 5$ for $\gamma^{(\alpha)}$ and Uniform on \mathcal{SP} for $\gamma^{(\beta)}$ (top panel) and Uniform prior on \mathcal{SP} for $\gamma^{(\beta)}$ and Ewens-Pitman prior with $\eta = 5$ for $\gamma^{(\alpha)}$ (bottom panel).

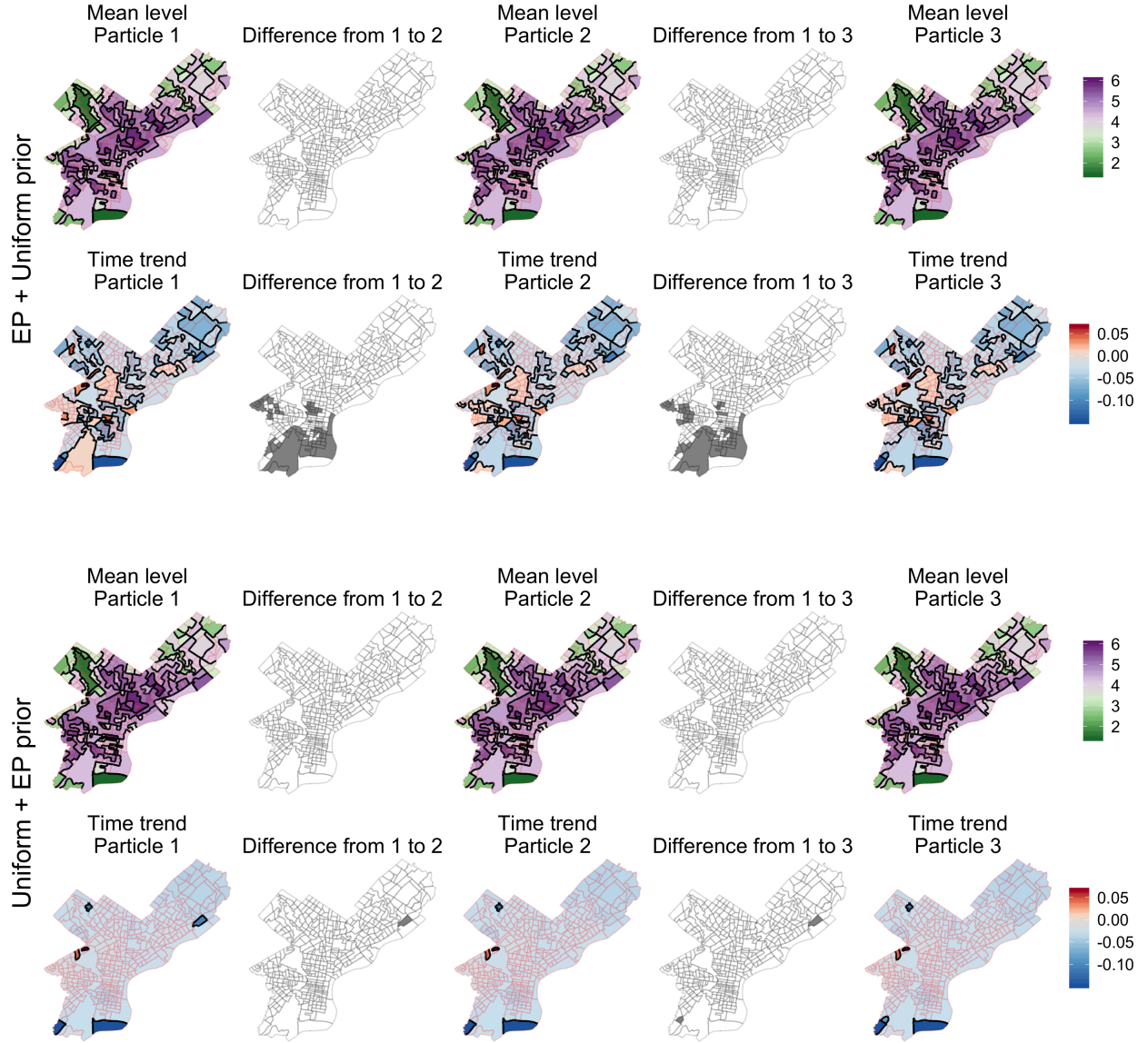


Figure S2: Colored plots: Top three models identified by our procedure. The thick borders represent the partition, and the color represents the posterior mean of the parameters α and β . Black and white plots: transition from the model on the left to the model on the right. The greyed areas represent the neighborhoods whose cluster assignments change in the partitions on the sides. **Top:** Ewens-Pitman prior with $\eta = 5$ for $\gamma^{(\alpha)}$ and Uniform on \mathcal{SP} for $\gamma^{(\beta)}$. **Bottom:** Uniform prior on \mathcal{SP} for $\gamma^{(\beta)}$ and Ewens-Pitman prior with $\eta = 5$ for $\gamma^{(\alpha)}$.

5 Derivation of Closed Form Expressions

5.1 One Partition Derivations

In Section 4, we considered a simpler model, in which we ignored the time trend and only focused on clustering the intercepts. That model was:

$$\begin{aligned}\boldsymbol{\gamma} &= \{S_1, \dots, S_K\} \sim \mathcal{P}_\gamma \\ \sigma^2 &\sim \text{Inv. Gamma} \left(\frac{\nu_\sigma}{2}, \frac{\nu_\sigma \lambda_\sigma}{2} \right) \\ \bar{\alpha}_k | \sigma^2 &\sim N(0, a_2 \sigma^2) \text{ for each } k = 1, \dots, K \\ \boldsymbol{\alpha}_{S_k} | \bar{\alpha}_k, \sigma^2 &\sim N_{n_k}(\bar{\alpha} \mathbf{1}_{n_k}, a_1 \sigma^2 \Sigma_k^{(\alpha)}) \text{ for each } k = 1, \dots, K \\ y_{i,t} | \alpha_i, \sigma^2 &\sim N(\alpha_i, \sigma^2) \text{ for each } i = 1, \dots, N, \text{ and } t = 1, \dots, T\end{aligned}$$

For the sake of completeness, we derive the corresponding marginal likelihood $p(\mathbf{y} | \boldsymbol{\gamma})$ and conditional expectation $\mathbb{E}[\boldsymbol{\alpha} | \boldsymbol{\gamma}, \mathbf{y}]$ for this simpler setting.

Now observe

$$\begin{aligned}p(\mathbf{y} | \boldsymbol{\alpha}, \sigma^2, \boldsymbol{\gamma}) &\propto \prod_{k=1}^K \prod_{i \in S_k} (\sigma^2)^{-\frac{T}{2}} \exp \left\{ -\frac{T(\bar{y}_i - \alpha_i)^2 + (T-1)s_i^2}{2\sigma^2} \right\} \\ &\propto (\sigma^2)^{-\frac{N(T-1)}{2}} \exp \left\{ -\frac{(T-1) \sum_{i=1}^N s_i^2}{2\sigma^2} \right\} \prod_{k=1}^K p(\bar{\mathbf{y}}_{S_k} | \boldsymbol{\alpha}_{S_k}, \sigma^2, \boldsymbol{\gamma})\end{aligned}$$

where $\bar{\mathbf{y}}_{S_k} | \boldsymbol{\alpha}_{S_k}, \sigma^2, \boldsymbol{\gamma} \sim N_{n_k}(\boldsymbol{\alpha}_{S_k}, T^{-1} \sigma^2 I_{n_k})$. From here, we conclude

$$p(\bar{\mathbf{y}} | \sigma^2, \boldsymbol{\gamma}) \propto (\sigma^2)^{-\frac{N(T-1)}{2}} \exp \left\{ -\frac{(T-1) \sum_{i=1}^N s_i^2}{2\sigma^2} \right\} \prod_{k=1}^K p(\bar{\mathbf{y}}_{S_k} | \sigma^2, \boldsymbol{\gamma})$$

To derive $p(\bar{\mathbf{y}}_{S_k} | \sigma^2, \boldsymbol{\gamma})$, we first note that marginally

$$\boldsymbol{\alpha}_{S_k} | \sigma^2 \sim N_{n_k}(0 \cdot \mathbf{1}_{n_k}, \sigma^2 [a_1 \Sigma_k^{(\alpha)} + a_2 \mathbf{1}_{n_k} \mathbf{1}_{n_k}^\top]).$$

Now marginalizing out $\boldsymbol{\alpha}_{S_k}$ we have

$$\bar{\mathbf{y}}_{S_k} | \sigma^2, \boldsymbol{\gamma} \sim N_{n_k} \left(0 \mathbf{1}_{n_k}, \sigma^2 \left[a_1 \Sigma_k^{(\alpha)} + a_2 \mathbf{1}_{n_k} \mathbf{1}_{n_k}^\top + T^{-1} I_{n_k} \right] \right)$$

Hence

$$\begin{aligned} p(\mathbf{y} | \sigma^2, \boldsymbol{\gamma}) &\propto (\sigma^2)^{-\frac{N(T-1)}{2}} \exp \left\{ -\frac{(T-1) \sum_{i=1}^N s_i^2}{2\sigma^2} \right\} \\ &\quad \times \prod_{k=1}^K (\sigma^2)^{-\frac{n_k}{2}} |\Omega_k^{(y)}|^{\frac{1}{2}} \exp \left\{ -\frac{1}{2\sigma^2} \sum_{k=1}^K \bar{\mathbf{y}}_k^\top \Omega_k^{(y)} \bar{\mathbf{y}}_k \right\} \end{aligned}$$

where $\Omega_k^{(y)} = [a_1 \Sigma_k^{(\alpha)} + a_2 \mathbf{1}_{n_k} \mathbf{1}_{n_k}^\top + T^{-1} I_{n_k}]^{-1}$.

Marginalizing out σ^2 , we conclude

$$p(\bar{\mathbf{y}} | \boldsymbol{\gamma}) = C(N, \nu_\sigma, \lambda_\sigma) \times \left(\prod_{k=1}^K |\Omega_k^{(y)}| \right)^{\frac{1}{2}} \times \left[\frac{\nu_\sigma \lambda_\sigma}{2} + \frac{1}{2} \sum_{k=1}^K \bar{\mathbf{y}}_k^\top \Omega_k^{(\alpha)} \bar{\mathbf{y}}_k + \frac{(T-1)}{2} \sum_{i=1}^N s_i^2 \right]^{-\frac{\nu_\sigma + NT}{2}}$$

We further compute

$$p(\bar{\mathbf{y}}_{S_k}, \boldsymbol{\alpha}_{S_k} | \sigma^2, \boldsymbol{\gamma}) \propto \exp \left\{ -\frac{1}{2\sigma^2} [\boldsymbol{\alpha}_{S_k}^\top V^{-1} \boldsymbol{\alpha}_{S_k} - 2 \boldsymbol{\alpha}_{S_k}^\top T \bar{\mathbf{y}}_{S_k}] \right\},$$

where $V^{-1} = \left[T I_{n_k} + \left(a_1 \Sigma_k^{(\alpha)} + a_2 \mathbf{1}_{n_k} \mathbf{1}_{n_k}^\top \right)^{-1} \right]$. From here, we immediate conclude that

$$\mathbb{E}[\boldsymbol{\alpha}_{S_k} | \bar{\mathbf{y}}_{S_k}, \boldsymbol{\gamma}] = T \times V \bar{\mathbf{y}}_{S_k}.$$

Finally, note that

$$\begin{aligned} p(\bar{\alpha}_k, \boldsymbol{\alpha}_{S_k}, \bar{\mathbf{y}}_{S_k} | \sigma^2, \boldsymbol{\gamma}) &\propto \exp \left\{ -\frac{1}{2\sigma^2} [(\bar{\mathbf{y}} - \boldsymbol{\alpha}_{S_k})^\top T (\bar{\mathbf{y}} - \boldsymbol{\alpha}_{S_k})] \right\} \\ &\quad \times \exp \left\{ -\frac{1}{2\sigma^2} [(\boldsymbol{\alpha}_{S_k} - \bar{\alpha}_k \mathbf{1}_{n_k})^\top a_1^{-1} \Omega_k^{(\alpha)} (\boldsymbol{\alpha}_{S_k} - \bar{\alpha}_k \mathbf{1}_{n_k})] \right\} \\ &\quad \times \exp \left\{ -\frac{1}{2\sigma^2} \bar{\alpha}_k^2 a_2^{-1} \right\} \end{aligned}$$

Therefore,

$$p(\bar{\alpha}_k | \boldsymbol{\alpha}_{S_k}, \bar{\mathbf{y}}, \sigma^2, \boldsymbol{\gamma}) \propto \exp \left\{ -\frac{1}{2\sigma^2} \left[\bar{\alpha}_k^2 \left(a_2^{-1} + a_1^{-1} \mathbf{1}_{n_k}^\top \Omega_k^{(\alpha)} \mathbf{1}_{n_k} \right) - 2\bar{\alpha}_k a_1^{-1} \mathbf{1}_{n_k}^\top \Omega_k^{(\alpha)} \boldsymbol{\alpha}_{S_k} \right] \right\}$$

By the Woodbury identity, we compute

$$\begin{aligned} \left[a_1 \Sigma_k^{(\alpha)} + a_2 \mathbf{1}_{n_k} \mathbf{1}_{n_k}^\top \right]^{-1} &= a_1^{-1} \Omega_k^{(\alpha)} - a_1^{-1} \Omega_k^{(\alpha)} \mathbf{1}_{n_k} \left[a_2^{-1} + a_1^{-1} \mathbf{1}_{n_k}^\top \Omega_k^{(\alpha)} \mathbf{1}_{n_k} \right]^{-1} \mathbf{1}_{n_k}^\top \Omega_k^{(\alpha)} a_1^{-1} \\ &= a_1^{-1} \Omega_k^{(\alpha)} - a_1^{-2} (1 - \rho)^2 \times \left[a_2^{-1} + a_1^{-1} (1 - \rho) n_k \right]^{-1} \times \mathbf{1}_{n_k} \mathbf{1}_{n_k}^\top \end{aligned}$$

So the posterior conditional mean of $\bar{\alpha}_k$ is given by

$$\mathbb{E}[\bar{\alpha}_k | \boldsymbol{\alpha}_{S_k}, \mathbf{y}_{S_k}, \boldsymbol{\gamma}] = \frac{a_1^{-1} \mathbf{1}^\top \Omega_k^{(\alpha)} \boldsymbol{\alpha}_{S_k}}{a_2^{-1} + a_1^{-1} \mathbf{1}_{n_k}^\top \Omega_k^{(\alpha)} \mathbf{1}_{n_k}} = \frac{a_1^{-1} (1 - \rho) \mathbf{1}_{n_k}^\top \boldsymbol{\alpha}_{S_k}}{a_2^{-1} + a_1^{-1} n_k (1 - \rho)}$$

Note: observe that as $a_2 \rightarrow \infty$ (i.e. as we allow the variability of the cluster means to increase), this conditional expectation converges to the $n_k^{-1} \mathbf{1}^\top \boldsymbol{\alpha}_{S_k}$, the arithmetic mean of the parameters within each block-group.

5.2 Two Partition Derivations

Recall from Section 2 that our full mode is:

$$\begin{aligned} \gamma^{(\alpha)}, \gamma^{(\beta)} &\sim \text{EP}(\eta; \mathcal{SP}) \\ \sigma^2 &\sim \text{IG} \left(\frac{\nu_\sigma}{2}, \frac{\nu_\sigma \lambda_\sigma}{2} \right) \\ (\bar{\alpha}_k)_k &\stackrel{iid}{\sim} N(0, a_2 \sigma^2) \\ (\bar{\beta}_{k'})_{k'} &\stackrel{iid}{\sim} N(0, b_2 \sigma^2) \\ (\boldsymbol{\alpha}_k)_k &\stackrel{ind}{\sim} \text{CAR}(\bar{\alpha}_k, a_1 \sigma^2, W_k^{(\alpha)}) \\ (\boldsymbol{\beta}_{k'})_{k'} &\stackrel{ind}{\sim} \text{CAR}(\bar{\beta}_{k'}, b_1 \sigma^2, W_{k'}^{(\beta)}) \\ (y_{i,t})_{i,t} &\stackrel{ind}{\sim} N(\alpha_i + \beta_i(t - \bar{t}), \sigma^2) \end{aligned}$$

We exploit the conditional conjugacy present in this model in several places. First, we have

closed form expressions for the conditional posterior means $\mathbb{E}[\boldsymbol{\alpha} \mid \mathbf{y}, \boldsymbol{\gamma}]$ and $\mathbb{E}[\boldsymbol{\beta} \mid \mathbf{y}, \boldsymbol{\gamma}]$, which we use in our particle optimization procedure to propose new transitions. Second, we can compute the marginal likelihood $p(\mathbf{y} \mid \boldsymbol{\gamma})$ in closed form, which we use to evaluate the optimization objective and pick between multiple transitions. Below, we carefully derive these closed form expressions, noting that in several places, we can avoid potentially expensive matrix inversions. In particular, the choice to center the time variable, thereby ensuring an orthogonal design matrix within each neighborhood, facilitates rapid likelihood evaluations.

Distribution of $\boldsymbol{\alpha}_k$ Let us first consider the vector of parameters $\boldsymbol{\alpha}_k$ in cluster $S_k^{(\alpha)}$ given σ^2 : by marginalizing the distribution of the grand cluster mean $\bar{\alpha}_k$, we find that its distribution is a multivariate normal with covariance matrix $\sigma^2 \Sigma_k^{(\alpha)}$, where $\Sigma_k^{(\alpha)} = a_1 \Sigma_{k,\text{CAR}}^{(\alpha)} + a_2 \mathbf{1}\mathbf{1}^\top = a_1 \left[\rho(W_k^{(\alpha)})^* + (1 - \rho)\mathbf{I} \right]^{-1} + a_2 \mathbf{1}\mathbf{1}^\top$. Note that its precision matrix can be computed using Woodbury's formula without having to invert any matrix:

$$\begin{aligned} (\Sigma_k^{(\alpha)})^{-1} &= a_1^{-1} \Omega_{k,\text{CAR}}^{(\alpha)} - a_1^{-1} \Omega_{k,\text{CAR}}^{(\alpha)} \mathbf{1} \left(a_1^{-1} \mathbf{1}^\top \Omega_{k,\text{CAR}}^{(\alpha)} \mathbf{1} + a_2^{-1} \right)^{-1} \mathbf{1}^\top a_1^{-1} \Omega_{k,\text{CAR}}^{(\alpha)} = \\ &= a_1^{-1} \Omega_{k,\text{CAR}}^{(\alpha)} - \frac{a_1^{-2} (1 - \rho)^2}{a_1^{-1} n_k (1 - \rho) + a_2^{-1}} \mathbf{1}\mathbf{1}^\top \end{aligned}$$

where $\Omega_{k,\text{CAR}}^{(\alpha)} = \left(\Sigma_{k,\text{CAR}}^{(\alpha)} \right)^{-1} = \rho(W_k^{(\alpha)})^* + (1 - \rho)\mathbf{I}$; the second line follows from noticing that $\mathbf{1}$ is both a left and right eigenvector of $\Omega_{k,\text{CAR}}^{(\alpha)}$ with eigenvalue $1 - \rho$. Similarly this holds for the distribution of $\boldsymbol{\beta}_{k'}$.

Distribution of $\boldsymbol{\alpha}$ Next, we can write the distribution of the whole vector $\boldsymbol{\alpha}$ given σ^2 and $\boldsymbol{\gamma}^{(\alpha)}$: by combining the distributions of the cluster specific parameters $\boldsymbol{\alpha}_k$'s, and using the independence between different clusters, we find that the distribution of $\boldsymbol{\alpha}$ given σ^2 and $\boldsymbol{\gamma}^{(\alpha)}$ is a multivariate normal with mean zero and covariance matrix that can be found by combining the $\Sigma_k^{(\alpha)}$'s. Because of the independence between clusters, *there exists an ordering of the indices of $\boldsymbol{\alpha}$* so that the covariance matrix of $\boldsymbol{\alpha} \mid \boldsymbol{\gamma}^{(\alpha)}, \sigma^2$ has a block-diagonal structure. We denote such permutation of the indices with $\pi^{(\alpha)}$, and it can be constructed by mapping the first n_1 elements to the indices in the first cluster ($\{\pi^{(\alpha)}(1), \dots, \pi^{(\alpha)}(n_1)\} = S_1^{(\alpha)}$), the following n_2 elements to the indices in the second cluster ($\{\pi^{(\alpha)}(n_1 + 1), \dots, \pi^{(\alpha)}(n_1 + n_2)\} = S_2^{(\alpha)}$), and so on. With such ordering, the k th diagonal block of the covariance matrix is $\sigma^2 \Sigma_k^{(\alpha)}$. Similarly, we can find a (potentially different) permutation $\pi^{(\beta)}$ for $\boldsymbol{\beta}$ and derive the

distribution of $\beta_\pi | \sigma^2, \gamma^{(\beta)}$.

Notation To describe the distributions of interest we can represent our model in the form of a unique linear model, by combining all the observations in a vector Y , combining the reordered coefficients in a unique vector $\theta = (\alpha_\pi, \beta_\pi)$ and appropriately constructing the covariate matrix X . In the next paragraphs we will provide with the details on how we constructed such vectors and matrix.

To build the column vector Y we stack the vectors \mathbf{y}_i with $i = 1, \dots, N$: Y is a vector of length $N \cdot T$ and each block of T rows corresponds to a particular neighborhood; in particular, the $((i-1)T + t)$ th entry of Y corresponds to $y_{i,t}$.

The vector of coefficients θ is found by concatenating the reordered α_π and β_π : for $i = 1, \dots, N$, elements $\theta_i = \alpha_{\pi^{(\alpha)}(i)}$ and $\theta_{N+i} = \beta_{\pi^{(\beta)}(i)}$.

The matrix of covariates X then has dimensions $NT \times 2N$; each block of T rows corresponds to a neighborhood and each column corresponds to an element of θ : the first N columns correspond to the elements of α_π and the second N columns to β_π . The rows of X corresponding to neighborhood i (rows $(i-1)T + t$ with $t = 1, \dots, T$) have an element equal to 1 in the $(\pi^{(\alpha)})^{-1}(i)$ th column, an element equal to $x_{it} = t - \bar{t}$ in the $(N + (\pi^{(\beta)})^{-1}(i))$ th column, and zero elsewhere. With such construction, the $(i-1)T + t$ row of the equation $Y = X\theta$ corresponds to $y_{i,t} = \theta_{(\pi^{(\alpha)})^{-1}(i)} + x_{it}\theta_{N+(\pi^{(\beta)})^{-1}(i)} = \alpha_i + (t - \bar{t})\beta_i$.

Marginal likelihood $Y | \gamma^{(\alpha)}, \gamma^{(\beta)}$ To recover the marginal likelihood $p(Y | \gamma^{(\alpha)}, \gamma^{(\beta)})$ we compute

$$\begin{aligned} & \int \left[\int p(Y | \alpha, \beta, \sigma^2) p(\alpha | \gamma^{(\alpha)}, \sigma^2) p(\beta | \gamma^{(\beta)}, \sigma^2) d\alpha d\beta \right] p(\sigma^2) d\sigma^2 = \\ &= \int \left[\int p(Y | \alpha_\pi, \beta_\pi, \sigma^2) p(\alpha_\pi | \gamma^{(\alpha)}, \sigma^2) p(\beta_\pi | \gamma^{(\beta)}, \sigma^2) d\alpha_\pi d\beta_\pi \right] p(\sigma^2) d\sigma^2 = \\ &= \int \left[\int p(Y | \theta, \sigma^2) p(\theta | \gamma^{(\alpha)}, \gamma^{(\beta)}, \sigma^2) d\theta \right] p(\sigma^2) d\sigma^2. \end{aligned}$$

Let us first compute $p(Y | \sigma^2, \gamma^{(\alpha)}, \gamma^{(\beta)}) = \int p(Y | \theta, \sigma^2) p(\theta | \gamma^{(\alpha)}, \gamma^{(\beta)}, \sigma^2) d\theta$. Using the notation for linear regression we can write $p(Y | \theta, \sigma^2) = N(X\theta, \sigma^2 \mathbf{I})$. The prior for θ is a normal distribution with mean zero and block covariance matrix Σ_θ : the first $n \times n$ block corresponds to the covariance matrix of α and the second to the one for β .

By integrating out $\boldsymbol{\theta}$, $p(Y|\gamma^{(\alpha)}, \gamma^{(\beta)}, \sigma^2) = N(\mathbf{0}, \sigma^2 \Sigma_Y)$ where $\Sigma_Y = \mathbf{I} + X \Sigma_\theta X^\top$. Its precision matrix can be computed using Woodbury's formula again: $\Sigma_Y^{-1} = \mathbf{I} - X(\Sigma_\theta^{-1} + X^\top X)^{-1} X^\top$. Note that $X^\top X$ is a diagonal matrix, and we derive its form at the end of this chapter.

The marginal likelihood can now be derived by integrating out σ^2 :

$$\begin{aligned} p(Y|\gamma^{(\alpha)}, \gamma^{(\beta)}) &= \int p(Y|\sigma^2, \gamma^{(\alpha)}, \gamma^{(\beta)}) p(\sigma^2) d\sigma^2 = \\ &= \pi^{-nT/2} \det(\Sigma_Y)^{-1/2} \frac{(\nu_\sigma \lambda_\sigma / 2)^{\nu_\sigma/2}}{\Gamma(\frac{\nu_\sigma}{2})} \int (\sigma^2)^{-\frac{NT+\nu_\sigma}{2}-1} e^{-\frac{Y^\top \Sigma_Y^{-1} Y + \nu_\sigma \lambda_\sigma}{2\sigma^2}} d\sigma^2 = \\ &= \pi^{-nT/2} \det(\Sigma_Y)^{-1/2} \frac{\Gamma(\frac{NT+\nu_\sigma}{2})}{\Gamma(\frac{\nu_\sigma}{2})} \left(\frac{\nu_\sigma \lambda_\sigma}{2}\right)^{\nu_\sigma/2} \left(\frac{\nu_\sigma \lambda_\sigma + Y^\top \Sigma_Y^{-1} Y}{2}\right)^{-(NT+\nu_\sigma)/2} = \\ &= \pi^{-nT/2} \det(\Sigma_Y)^{-1/2} \frac{\Gamma(\frac{NT+\nu_\sigma}{2})}{\Gamma(\frac{\nu_\sigma}{2})} \left(\frac{\nu_\sigma \lambda_\sigma}{2}\right)^{-NT/2} \left(1 + \frac{Y^\top \Sigma_Y^{-1} Y}{\nu_\sigma \lambda_\sigma}\right)^{-(NT+\nu_\sigma)/2}. \end{aligned}$$

Note that if $\lambda_\sigma = 1$, this is multivariate t-distribution with ν_σ degrees of freedom.

For this we need to compute the quadratic form

$$Y^\top \Sigma_Y^{-1} Y = Y^\top Y - Y^\top X (\Sigma_\theta^{-1} + X^\top X)^{-1} X^\top Y.$$

Because of the block diagonal structure of $\Sigma_\theta^{-1} + X^\top X$ we can write this as a sum over the clusters of the two partitions. Consider the column vector $X^\top Y$ of length $2N$: the first N elements correspond to the summary statistics related to the $\alpha_{\pi(i)}$'s and we will denote the ones corresponding to cluster $S_k^{(\alpha)}$ with $(X^\top Y)_k^{(\alpha)}$, while the second N elements are for the β_i 's and we denote with $(X^\top Y)_{k'}^{(\beta)}$ the ones for cluster $S_{k'}^{(\beta)}$. Now we can write

$$\begin{aligned} Y^\top X (\Sigma_\theta^{-1} + X^\top X)^{-1} X^\top Y &= \sum_{k=1}^{K^{(\alpha)}} (X^\top Y)_k^{(\alpha)\top} ((\Sigma_k^{(\alpha)})^{-1} + T\mathbf{I})^{-1} (X^\top Y)_k^{(\alpha)} \\ &\quad + \sum_{k'=1}^{K^{(\beta)}} (X^\top Y)_{k'}^{(\beta)\top} ((\Sigma_{k'}^{(\beta)})^{-1} + \sum x_t^2 \mathbf{I})^{-1} (X^\top Y)_{k'}^{(\beta)} \end{aligned}$$

where $(\Sigma_k^{(\alpha)})^{-1} + T\mathbf{I}$ is the diagonal blocks of $\Sigma_\theta^{-1} + X^\top X$ corresponding to cluster $S_k^{(\alpha)}$ and $(\Sigma_{k'}^{(\beta)})^{-1} + \sum x_t^2 \mathbf{I}$ corresponds to $S_{k'}^{(\beta)}$; each of them can be inverted using methods for symmetric positive definite matrices.

To compute the marginal likelihood we are left we calculating the determinant of Σ_Y , where

we can use the reciprocal of the determinant of its inverse

$$\det(\Sigma_Y^{-1}) = \det(\mathbf{I} - X(\Sigma_\theta^{-1} + X^\top X)^{-1} X^\top) = \det(\mathbf{I} - (\Sigma_\theta^{-1} + X^\top X)^{-1} X^\top X)$$

where the last equality is given by Sylvester's formula, and allows us to compute the determinant of a smaller dimensional matrix. Moreover, because of its block diagonal structure, we can compute the determinant block-wise.

Posterior mean of α, β The calculations for the posterior mean of α, β are very similar: using the same notation and the results for linear regression, we can find

$$\mathbb{E}[\theta|Y, \gamma^{(\alpha)}, \gamma^{(\beta)}, \sigma^{-1}] = (X^\top X + \Sigma_\theta^{-1})^{-1} X^\top Y$$

and since this does not depend on σ^2 , it coincides with $\mathbb{E}[\theta|Y, \gamma^{(\alpha)}, \gamma^{(\beta)}]$. Because of the block diagonal structure of the matrices involved, we can compute the estimate of the parameter for each cluster independently. Moreover, note that the inverse of $X^\top X + \Sigma_\theta^{-1}$ is computed in the likelihood calculation, so it can be stored and does not need to be computed two times.

Derivation of $X^\top X$ Since in our formulation the covariates are orthogonal, i.e. $\sum_{t=1}^T x_{it} = 0$ for all i , $X^\top X$ is a diagonal matrix. Note that column $X_{(\pi^{(\alpha)})^{-1}(i')}$ contains T 1's in rows $t + (i' - 1) \times T$ and zeros elsewhere; similarly column $X_{N+(\pi^{(\beta)})^{-1}(i')}$ contains elements $(x_{i't})$ in rows $t + (i' - 1) \times T$ and zero's elsewhere. Thus, when we compute $(X^\top X)_{ij}$ we consider the cross product of columns X_i and X_j . Depending on the value of i and j , we have the following cases:

- if $i = j \leq N$, then $(X^\top X)_{ij} = T$,
- if $i = j \geq N$, then $(X^\top X)_{ij} = \sum_t x_{\pi^{(\beta)}(j-N),t}^2$,
- if $i \leq N$ and $j = N + i$, then $(X^\top X)_{ij} = \sum_t x_{\pi^{(\beta)}(i),t} = 0$,
- if $j \leq N$ and $i = N + j$, then $(X^\top X)_{ij} = \sum_t x_{\pi^{(\beta)}(j),t} = 0$,
- for any other i, j , $(X^\top X)_{ij} = 0$.

Thus the matrix $X^\top X$ is a diagonal matrix: the first $n \times n$ diagonal block is $T\mathbf{I}$, and the second diagonal block is a diagonal matrix whose entries are $\sum_{t=1}^T x_{it}^2$; when we have fixed

design, $x_{it} = x_t = t - \bar{t}$, then $\sum_{t=1}^T x_{it}^2 = \sum_{t=1}^T (t - \bar{t})^2$ is constant, so the second diagonal block is $\sum x_{it}^2 \mathbf{I}$. Because of the orthogonality of the covariates, the upper-right and lower-left blocks are zero matrices, since $\sum_{t=1}^T x_{it} = 0$.

Note on cluster-wise update of calculations. In our greedy search when we perform a move only one or two clusters in only one partition is changed: in a *split* move for $\gamma^{(\cdot)}$, a cluster is divided into two sub-clusters, and the original cluster replaced by the first, while the second creates an additional cluster; in a *merge* move, one of two clusters is deleted and the other is replaced to the merge of the two original clusters. In each case, we need to update the value of the marginal likelihood, of the prior for $\gamma^{(\cdot)}$ and of the estimate of the parameters.

Because of the block structure given by orthogonality of covariates and by the reordering of the parameters, changing the structure of some clusters does not affect the parameter estimates for other clusters that are not involved in the move. This implies that updates for updates to $S_k^{(\alpha)}$ do not affect the parameter estimates α_h for $h \neq k$ or $\beta_{k'}$ for any k' . Similarly, since the quadratic form $Y^\top \Sigma_Y^{-1} Y$ can be written as sum of cluster-specific quadratic forms, we can update only the quadratic form of the clusters affected and we can compute the determinant of the blocks of Σ_Y corresponding to the modified clusters.

This allows us to invert matrices that scale like the size of the clusters, reducing the computational costs dramatically.